RESEARCH ARTICLE

PARP1-Driven Poly-ADP-Ribosylation Regulates BRCA1 Function in Homologous Recombination–Mediated DNA Repair

Yiduo Hu[1,2,3], Sarah A. Petit[1,2], Scott B. Ficarro[1,4,5], Kimberly J. Toomire[1,2], Anyong Xie[6], Elgene Lim[7], Shiliang A. Cao[7], Eunyoung Park[1,4], Michael J. Eck[1,4], Ralph Scully[6], Myles Brown[7], Jarrod A. Marto[1,4,5], and David M. Livingston[1,2,3]

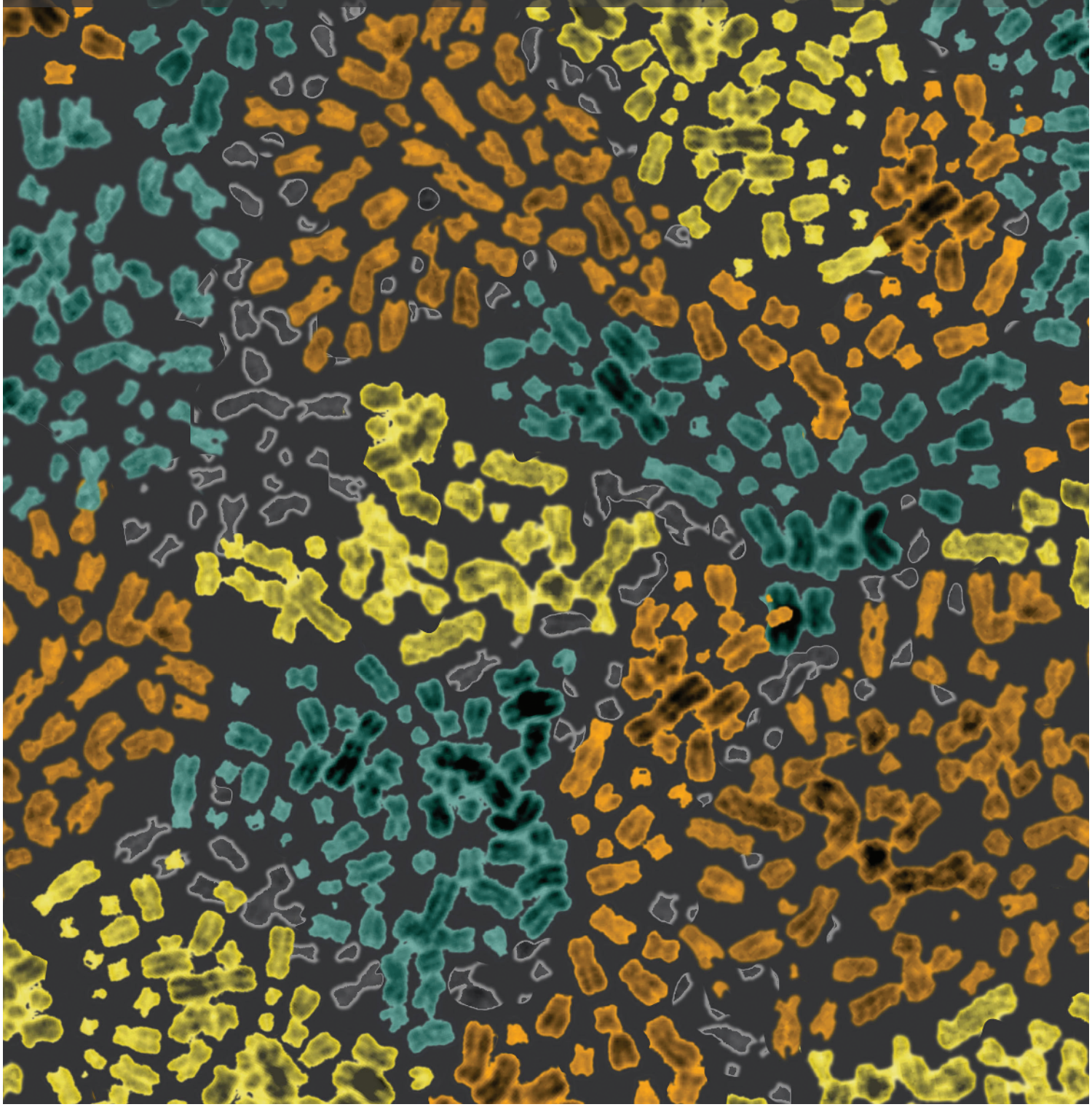

ABSTRACT BRCA1 promotes homologous recombination–mediated DNA repair (HRR). However, HRR must be tightly regulated to prevent illegitimate recombination. We previously found that BRCA1 HRR function is regulated by the RAP80 complex, but the mechanism was unclear. We have now observed that PARP1 interacts with and poly-ADP-ribosylates (aka PARsylates) BRCA1. PARsylation is directed at the BRCA1 DNA binding domain and downmodulates its function. Moreover, RAP80 contains a poly-ADP-ribose–interacting domain that binds PARsylated BRCA1 and helps to maintain the stability of PARP1–BRCA1–RAP80 complexes. BRCA1 PARsylation is a key step in BRCA1 HRR control. When BRCA1 PARsylation is defective, it gives rise to excessive HRR and manifestations of genome instability. BRCA1 PARsylation and/or RAP80 expression is defective in a subset of sporadic breast cancer cell lines and patient-derived tumor xenograft models. These observations are consistent with the possibility that such defects, when chronic, contribute to tumor development in *BRCA1*$^{+/+}$ individuals.

SIGNIFICANCE: We propose a model that describes how BRCA1 functions to both support and restrict HRR. BRCA1 PARsylation is a key event in this process, failure of which triggers hyper-recombination and chromosome instability. Thus, hyperfunctioning BRCA1 can elicit genomic abnormalities similar to those observed in the absence of certain BRCA1 functions. *Cancer Discov; 4(12); 1430–47. ©2014 AACR.*

INTRODUCTION

BRCA1 is a breast and ovarian cancer–suppressing gene and a major contributor to genome integrity control. The latter function is a major component of its tumor-suppressing function (1, 2). Among its various DNA damage response functions, BRCA1 normally promotes error-free, homologous recombination–type, DNA damage repair (HRR). Defects in this pathway lead to DNA damage and genomic instability. Strong genetic and epidemiologic links exist between BRCA1 HRR function and its breast cancer suppression activity (3–6). Yet, how these phenomena are mechanistically connected is poorly understood.

Recent studies, including some from our group, showed that at least four BRCA1-containing nuclear protein complexes concentrate in double-strand break (DSB)–containing nuclear foci (e.g., ionizing radiation–induced foci, or IRIF) and participate in these structures in the HRR pathway (7–11). One of these, the RAP80 (aka UIMC1)–BRCA1 complex, regulates the concentration in IRIF of two HRR-promoting (pro-HRR), BRCA1-containing protein complexes [i.e., the CtIP (CtBP-interacting protein, aka RBBP8)–BRCA1 and BACH1 (aka BRIP1/FANCJ)–BRCA1 complexes]. BRCA1 employs this mechanism in a process that maintains a physiologic amplitude of HR-mediated DSB repair. Loss of amplitude regulation (aka tuning) after RAP80 depletion leads to excessive DSB end resection and the type of chromosomal instability that, when chronic, is associated with breast and ovarian cancer development (12, 13).

Here, we report that PARP1 is a physiologic, RAP80- and BRCA1-associated protein and that its ability to operate as a poly-ADP-ribosyl transferase (pADRT) supports proper HRR tuning. More specifically, in this process, PARP1 poly-ADP-ribosylates (aka PARsylates) BRCA1, targeting its DNA binding domain and reducing its avidity for DNA. BRCA1 PARsylation is required for maintenance of the stability of the RAP80–BRCA1–PARP1 complex. Moreover, RAP80 contains a PAR-interacting domain (PID) that binds PARsylated BRCA1. This, in turn, enables fine-tuning of BRCA1 HRR function. A major outcome of this process is a BRCA1-driven contribution to chromosome integrity control.

RESULTS

PARP1 Is a Partner of the RAP80–BRCA1 Complex

Using crosslinking-assisted tag affinity purification, we identified a number of novel binding partners of the tagged RAP80–BRCA1 complex in HeLa S3 cells ($N = 95$; Supplementary Fig. S1A and S1B and see Supplementary Information for a detailed description of the method). These proteins can be portrayed as a network of communicating polypeptides,

[1]Department of Cancer Biology, Dana-Farber Cancer Institute, Boston, Massachusetts. [2]Department of Genetics, Harvard Medical School, Boston, Massachusetts. [3]Department of Medicine, Brigham and Women's Hospital, Boston, Massachusetts. [4]Department of Biological Chemistry and Molecular Pharmacology, Harvard Medical School, Boston, Massachusetts. [5]Blais Proteomics Center, Dana-Farber Cancer Institute, Boston, Massachusetts. [6]Department of Medicine, Beth Israel Deaconess Medical Center, Boston, Massachusetts. [7]Department of Medical Oncology, Dana-Farber Cancer Institute, Boston, Massachusetts.

Note: Supplementary data for this article are available at Cancer Discovery Online (http://cancerdiscovery.aacrjournals.org/).

Current address for S.A. Petit: Karmanos Cancer Institute, Detroit, Michigan; current address for A. Xie: Sir Run Run Shaw Hospital and Institute of Translational Medicine, Zhejiang University, Hangzhou, Zhejiang, China; current address for E. Lim: Ludwig Cancer Research and Olivia Newton John Cancer and Wellness Centre, West Heidelberg, Victoria, Australia.

Corresponding Author: David M. Livingston, Dana-Farber Cancer Institute, 450 Brookline Avenue, Boston, MA 02215. Phone: 617-632-3074; Fax: 617-632-4381; E-mail: david_livingston@dfci.harvard.edu

doi: 10.1158/2159-8290.CD-13-0891

based upon their gene ontology terms and their experimentally deciphered protein interaction properties (14). Among their interacting partners are proteins recently shown to be involved in cellular responses to DSBs, including SFPQ (15), CHD4 (16), and UBR5 (ref. 17; Supplementary Fig. S1C).

Interestingly, PARP1 was identified as one such RAP80–BRCA1 partner (Supplementary Fig. S1C and S1D). Results of a gel filtration experiment showed that PARP1 was detected in a wide range of fractions, including those containing BRCA1, RAP80, and ABRAXAS (ABRA1), another component of the RAP80 complex (Supplementary Fig. S1E). These results suggest that a fraction of the detected PARP1 is associated with the RAP80–BRCA1 complex.

We also detected an interaction between PARP1 and RAP80–BRCA1 by endogenous/endogenous co-immunoprecipitation (co-IP) performed in the absence of a cross-linking agent. As shown in Fig. 1A and B, endogenous PARP1 associated with endogenous BRCA1, RAP80, and ABRA1. PARP1 was also detected in endogenous BRCA1 IPs (Fig. 1C). Similar interactions between endogenous proteins were detected in co-IP experiments performed with other cell lines (e.g., U2OS, T98G, and 293T cells). The same co-IP results were detected in cell lysates treated with ethidium bromide, implying that the association between these proteins is not a result of nucleic acid bridging (Supplementary Fig. S1F; ref. 18).

PARP1 Promotes BRCA1 PARsylation

Interestingly, BRCA1 bands that smeared and migrated more slowly than normal BRCA1 p220 were detected in anti-PARP1 IPs (Fig. 1B). This suggested that the BRCA1 species that exist in complex with PARP1 are modified. To test whether these modified forms of BRCA1 represent PARsylated BRCA1, we performed co-IP with anti–poly-ADP-ribose (PAR) antibodies. Multiple BRCA1 bands that migrated more slowly than unmodified BRCA1 appeared in these IPs [Fig. 1C (lanes 5 and 6, a mouse monoclonal anti-PAR antibody was used in these IPs) and Fig. 1D (lanes 3 and 4, a rabbit polyclonal anti-PAR antibody was used in these IPs)]. Similar results were obtained when other cell lines were examined, including U2OS, T98G, 293T, MCF7, and telomerase-immortalized, primary mammary epithelial cells (iMEC), and when three different anti-BRCA1 antibodies were used (Supplementary Fig. S1G and data not shown).

Poly-ADP-ribose glycohydrolase (PARG) cleaves conjugated ADP-ribose polymers (19). In anti-PAR immunoprecipitates from a cell lysate that was exposed to purified PARG, the smear detected with an anti-BRCA1 antibody was greatly reduced (Fig. 1E). Thus, the modified, slowly migrating, anti–PAR-reactive BRCA1 species are PARsylated.

To test whether PARP1 is the enzyme that catalyzes BRCA1 PARsylation, a *Parp1*$^{-/-}$ strain of mouse embryonic fibroblasts (MEF; ref. 20) was analyzed before and after reconstitution with a full-length human *PARP1* cDNA (or with the empty vector as control). Much stronger signals of PARsylated mouse BRCA1 were consistently detected in PARP1-reconstituted cells than in control cells, and the difference was particularly strong after ionizing radiation (IR; Fig. 1F, lanes 1 and 2). Thus, PARP1 likely catalyzes the vast majority of BRCA1 PARsylation in response to DNA damage. Some weak, anti–PAR-reactive BRCA1 bands were seen in vector-transfected cells, suggesting that other PARPs are responsible for a small fraction of BRCA1 PARsylation (Fig. 1F, lanes 3 and 4 of the top plot; refs. 21, 22). However, these data indicate that BRCA1 is primarily PARsylated by PARP1.

BRCA1 promotes HR-mediated DNA repair in S and G_2 phases, using undamaged sister chromatids as templates (23, 24). Thus, we asked whether cell-cycle state influences BRCA1 PARsylation. In synchronized T98G cells irradiated at various time points after release from G_0, PARsylated BRCA1 was apparent throughout the cell cycle (Supplementary Fig. S1H). However, we observed the most significant increase in PARsylated BRCA1 between 16 and 24 hours after G_1 release, when the largest proportion of cells were in S and G_2 (i.e., S+G2 cells had increased from 11% to 70% of the total population; Supplementary Fig. S1H, lanes 4 and 5). From 24 to 32 hours, when most cells had entered the next G_1 (i.e., G_1 increased from 30% to 65%), the PARsylated BRCA1 signal decreased significantly (Supplementary Fig. S1H, lane 6). Thus, BRCA1 is most heavily PARsylated during the period in which it exerts its HRR-related functions (i.e., S and G_2).

Because PARP1 is abundant and stable, the possibility that the observed PARsylation of BRCA1 occurs after cell extraction was raised. However, adding 10 μmol/L olaparib (a PARP1 inhibitor with an IC_{50} of ~5 nmol/L; ref. 25) to the cell lysate did not affect the detection of BRCA1 PARsylation (Supplementary Fig. S1I).

Similarly, when permeabilized cells were briefly incubated (30 minutes) with a reaction buffer containing 12.5 μmol/L biotinylated nicotinamide adenine dinucleotide (bio-NAD) as substrates for PARsylation and then lysed under denaturing conditions (Fig. 1G), BRCA1 was detected in streptavidin-reactive precipitates (Fig. 1H, top plot, lane 3). As a positive control, histone H2B, a known substrate of PARP1 (26), was also found to label with biotin in this assay (Fig. 1H, bottom, lane 3). In contrast, preincubating cells with olaparib abolished these PARsylation events (Fig. 1H, lane 4). These results further confirm that a fraction of endogenous BRCA1 is PARsylated in cells.

BRCA1 PARsylation Is Directed at Its DNA Binding Domain and Controlled by an Internal Sequence

We attempted to determine which segments of BRCA1 are targeted by this modification. Given that mass spectrometry analyses of full-length BRCA1 were uninformative (see Supplementary Information), we asked whether any of a collection of different GST-BRCA1 p220 fragments that, collectively, represent the entire protein are PARsylated by PARP1 in a cell-free assay (see Supplementary Information). We found that the reaction primarily targeted one fragment, i.e., F3.7 = aa 501–744 (Supplementary Fig. S2A–S2F). This fragment is encoded by *BRCA1* exon 11 (Fig. 2A). Of note, F3.7 contains sequences that support both BRCA1 nuclear localization (27, 28) and its DNA binding activity (29–32; Fig. 2A).

We next asked whether BRCA1 PARsylation results in PAR being conjugated to a specific residue(s) in F3.7. However, after extensive analyses, it appeared that PAR was directed to a number of sites in the F3.7 region (see details in Supplementary Fig. S3A–S3D and Supplementary Information). Such nonunique mono- or poly-ADP-ribose modifications—some

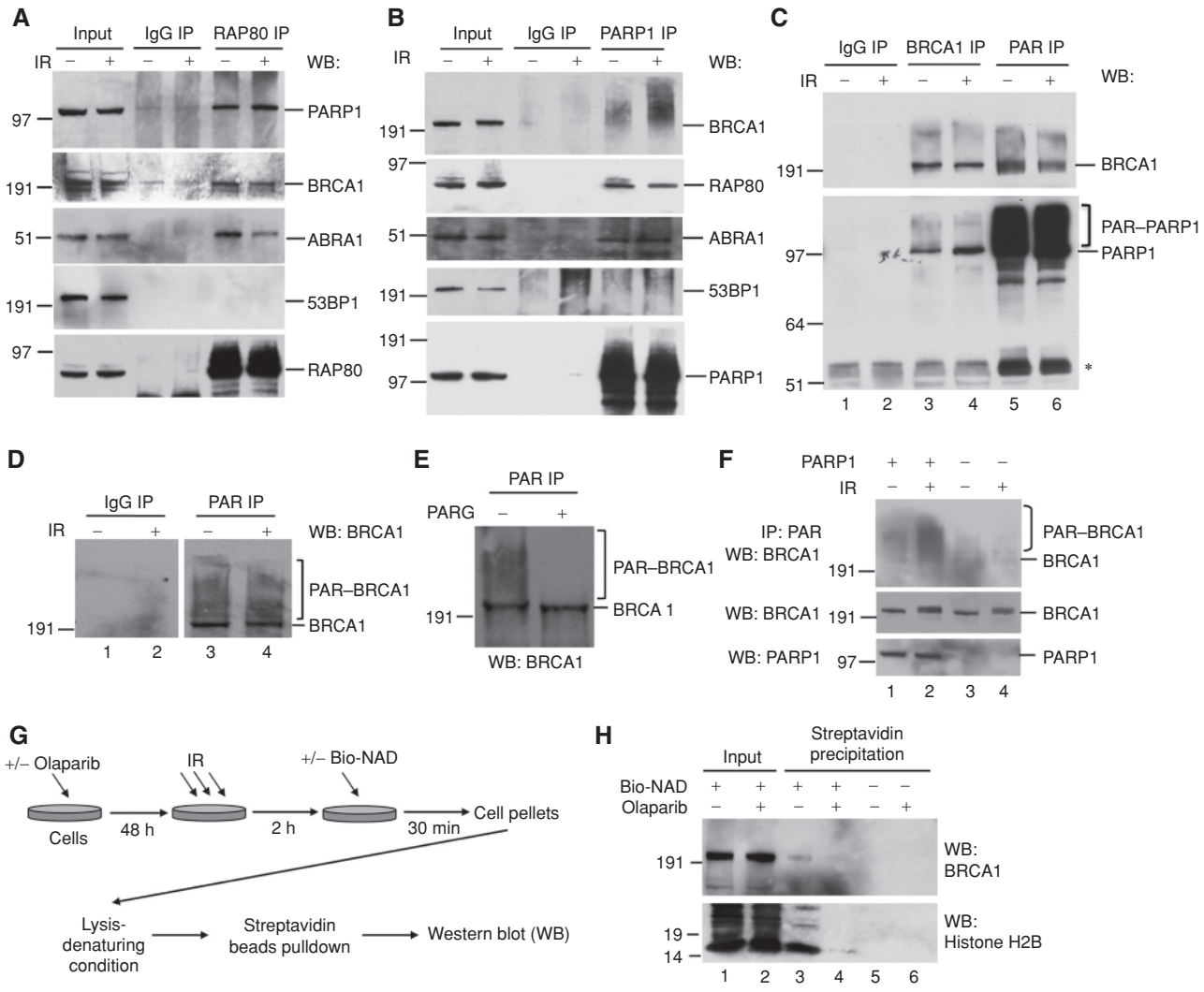

Figure 1. PARP1 is a partner of the RAP80–BRCA1 complex and promotes BRCA1 PARsylation. **A,** HeLa cells were exposed to 10 Gy IR or mock treated and lysed 4 hours later. IP was performed with a rabbit polyclonal anti-RAP80 antibody or IgG control. The IPs were blotted, and the blots were probed with antibodies to PARP1, BRCA1, ABRA1, 53BP1, or RAP80. Five percent of total cell lysate was blotted as an input control in all IP experiments. **B,** HeLa cells were treated as described in **A.** IPs were generated with a monoclonal anti-PARP1 antibody or IgG control, blotted, and the blots were probed with antibodies to BRCA1, RAP80, ABRA1, 53BP1, or PARP1. **C,** HeLa cells were treated as described in **A**. IPs were generated with a rabbit polyclonal anti-BRCA1 antibody, or a monoclonal anti-PAR antibody, or IgG control, blotted, and the blots were probed with antibodies to BRCA1 or PARP1. *, migration position of IgG heavy chain. **D,** HeLa cells were treated as described in **A**. IPs were generated with a rabbit polyclonal anti-PAR antibody or an IgG control and blotted, and the blots were probed with a monoclonal antibody to BRCA1. **E,** HeLa cells were treated, and anti-PAR IPs were performed as described in **D**. Immunoprecipitated proteins were eluted and then incubated with PARG or with buffer only. Proteins were then blotted and probed with a BRCA1 antibody. **F,** *Parp1*$^{-/-}$ MEFs were stably reconstituted with human *PARP1* cDNA or empty vector. Cells were treated with 10 Gy IR or mock treated and then lysed after 2 hours of recovery. IPs were performed with an anti-PAR antibody and then probed with an antibody directed against mouse BRCA1. Input proteins were blotted directly and probed with antibodies recognizing PAR (a different antibody from that used in the PAR IP), mouse BRCA1, or PARP1. **G** and **H,** *in vivo* incorporation of biotinylated-NAD (bio-NAD). **G,** a schematic diagram showing the experimental procedure (see details in Methods). **H,** Western blots (WB) showing that BRCA1 and Histone H2B were detected in streptavidin precipitates, whereas olaparib pretreatment blocked bio-NAD incorporation. Total proteins (20 μg) were loaded as an input control.

within discrete/specific protein domains—have been described for other proteins (for reviews, see refs. 33–35).

Given that the F3.7 region rather than specific residues within it was targeted for PARsylation, we asked whether there is a dedicated F3.7 sequence that targets PARsylation to this region. We focused on 10 nonoverlapping segments of F3.7, each composed of eight residues. This is because, collectively, they encompass the most evolutionarily conserved region within this BRCA1 segment (refs. 36, 37; Fig. 2A and Supplementary Figs. S3C, SD1–SD10). The question was whether deletion of any of them from F3.7 affects its ability to be mono- and/or poly-ADP-ribosylated.

Repeatedly, internal deletion of the D5 segment, which contains BRCA1 p220 residues 611–618 (LRRKSSTR), inhibited both cell-free mono- and poly-ADP-ribosylation of otherwise intact F3.7 (Supplementary Fig. S3E). Moreover, mass

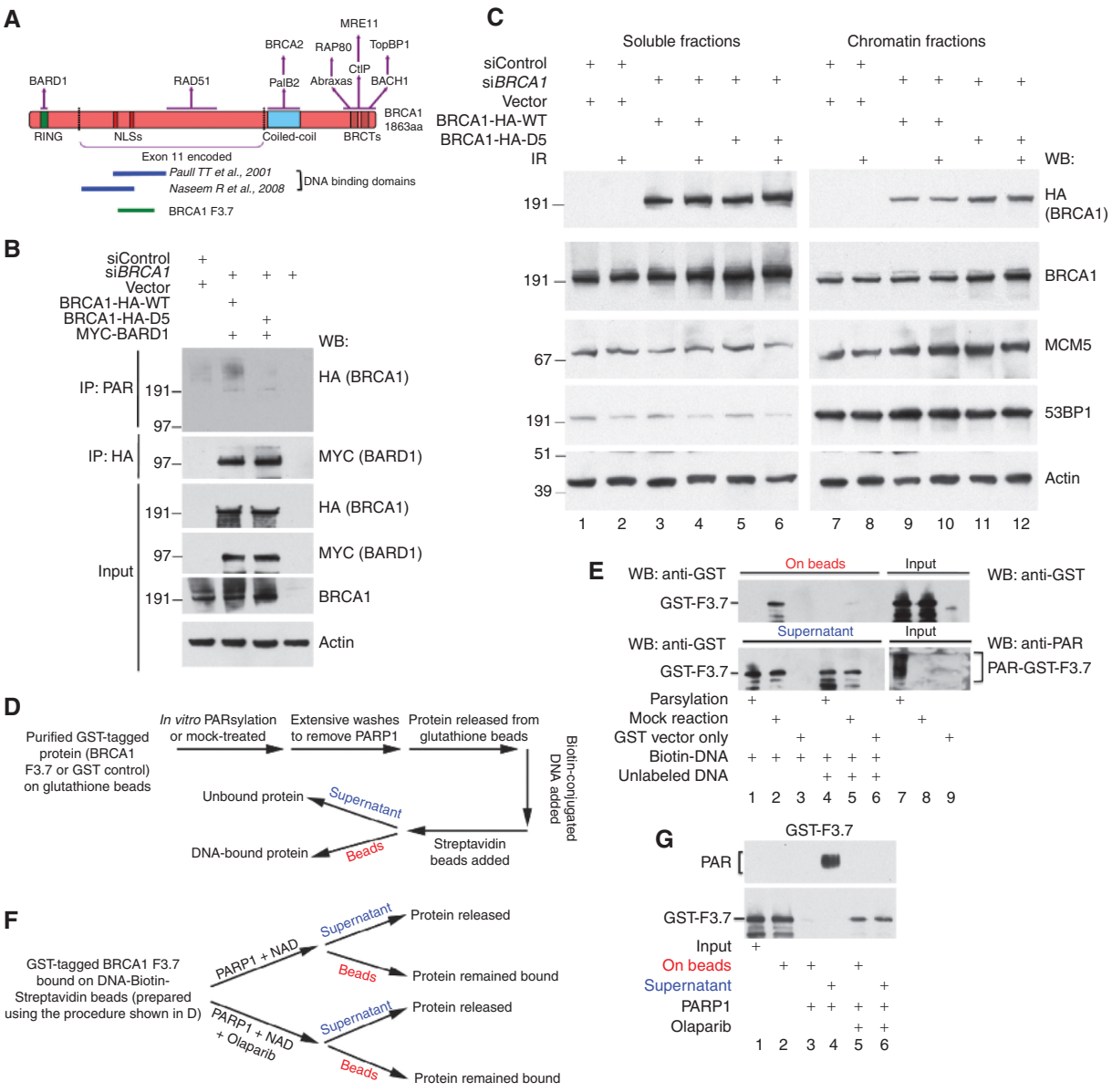

Figure 2. PARsylation modulates BRCA1 DNA binding activity. **A,** a schematic diagram showing elements of the domain structure of human BRCA1 p220. Domains are labeled under the protein diagram, whereas some of their respective binding partners are indicated above. The section indicated between the two dotted lines is encoded by *BRCA1* exon 11. The dark blue lines indicate previously mapped regions required for BRCA1 DNA binding activity. The green line shows the location of BRCA1 fragment F3.7, which is targeted by PARsylation. **B,** the BRCA1-D5 mutant is defective for PARsylation in cells. The 293T cells were sequentially transfected with the indicated combinations of control siRNA or *BRCA1* siRNA and *BRCA1* siRNA–resistant wild-type (WT) or D5 mutant cDNA or *BRCA1* siRNA only. Forty-eight hours later, cells were irradiated with 10 Gy IR and lysed after 2 hours. IPs were performed with an anti-PAR or an anti-HA antibody (recognizing HA-tagged BRCA1). Immunoprecipitated proteins were blotted, and the blots were probed with HA or MYC antibody (recognizing MYC-tagged BARD1), respectively. Input samples were blotted, and the blots were probed with HA, MYC, BRCA1 (recognizing endogenous and HA-tagged BRCA1), or actin antibody. **C,** the BRCA1-D5 mutant exhibits stronger association with chromatin fractions compared with BRCA1-WT. The 293T cells transfected with either control or *BRCA1* siRNA were subsequently transfected with vector, siRNA-resistant BRCA1-WT, or siRNA-resistant BRCA1-D5, as indicated. Forty-eight hours later, cells were irradiated with 10 Gy IR and collected after 4 hours. Cells were processed for extraction to separate soluble and chromatin fractions. Equivalent amounts of lysate protein derived from each fraction were blotted, and the blots were probed with HA, BRCA1 (endogenous), MCM5, 53BP1, or actin antibody. **D** and **E,** PARsylation of BRCA1 F3.7 abolished its DNA binding activity *in vitro*. **D,** a schematic diagram showing the experimental procedure. For details, please see Methods. **E,** DNA-bound (on beads) and unbound (supernatant) proteins were detected by Western blotting, using an anti-GST antibody (lanes 1–6). Equivalent amounts of modified (PAR) and unmodified proteins to those used in the DNA binding assay were loaded as input samples (lanes 7–9, top). PARsylation was confirmed with an anti-PAR antibody (lanes 7–9, bottom). **F** and **G,** PARP1-driven PARsylation released DNA-bound F3.7. **F,** a schematic diagram showing the experimental procedure. For details, please see Methods. **G,** input (lane 1) and equivalent amount of DNA-bound GST-F3.7 were mock treated (lane 2) or incubated with PARP1 in the absence (lanes 3 and 4) or presence of olaparib (lanes 5 and 6). Released protein (supernatant, lanes 4 and 6) and protein still bound to DNA (on beads, lanes 2, 3, and 5) were blotted and probed with an anti-GST antibody. The presence of PARsylated proteins in the supernatant of PARP1-treated sample (lane 4) was detected by probing the same membrane with an anti-PAR antibody (top).

spectrometry (MS) analysis performed on peptides derived from Glu-C digestion of mono-ADP-ribosylated BRCA1 F3.7 (see Supplementary Information) identified only unmodified D5 peptides, suggesting that the D5 sequence itself lacks ADP-ribosyl–conjugating sites (data not shown).

More importantly, PARsylation of a full-length, wild-type (WT) BRCA1 polypeptide lacking D5 (BRCA1-D5) was also markedly diminished in cells (Fig. 2B). Although BRCA1-D5 was only minimally PARsylated, it is nuclear and appeared to interact normally with BARD1 (Fig. 2B, second plot from the top). It also concentrated in IRIF in S–G_2 phase cells, like endogenous WT BRCA1 (Supplementary Fig. S4), and it interacted normally with the BRCA1 partners CtIP and BACH1 (please see below). Thus, the BRCA1-D5 mutant exhibited normal BRCA1 properties, including nuclear localization and interactions with important partner proteins. However, it cannot be properly PARsylated.

PARsylation Modulates BRCA1 DNA Binding Activity

Because PARsylation targets a BRCA1 region that partially overlaps the previously mapped BRCA1 DNA binding domains (Fig. 2A), we asked whether PARsylation influences BRCA1 DNA binding activity. Indeed, when two cell lines, each containing a single, genome-integrated I-*Sce*I HRR repair reporter, were treated with olaparib, the amount of endogenous BRCA1 associated with chromatin near the breakage site increased significantly, as measured by chromatin immunoprecipitation (ChIP) assay (Supplementary Fig. S5A and S5B). The avidity of BRCA1 for these two DSB-containing loci differed, even in the absence of olaparib. Conceivably, this is due to the different location of each locus in the genome.

Although these results suggest strongly that PARsylation modulates BRCA1 DNA binding after DNA damage in cells, we could not exclude the possibility that global inhibition of PARsylation by olaparib may disturb other factors, such as certain chromatin structures that might indirectly affect BRCA1 binding. We attempted to circumvent this complication by analyzing the non-PARsylatable BRCA1-D5 and its WT counterpart. Although we observed a small but reproducible increase in the amount of chromatin-associated BRCA1 in cells transiently expressing BRCA1-D5, compared with cells transiently expressing BRCA1-WT at comparable levels (Fig. 2C, compare lanes 11 and 12 with lanes 9 and 10), we found no consistent difference in chromatin binding between BRCA1-WT and BRCA1-D5 in such cells by ChIP (data not shown). Because only a small fraction of BRCA1 is PARsylated at any time and this modification may turn over rapidly (cf. Fig. 1D and H), we may have been unable to detect the subtle and transient difference in chromatin binding between BRCA1-WT and BRCA1-D5 in response to a single DSB in these cells.

However, because BRCA1 preferentially binds four-way junction-structured DNA that exhibits certain features of a recombination intermediate *in vitro* (29, 32), we asked whether BRCA1 F3.7 manifests such an activity and whether it could be modulated by PARsylation. As shown in Fig. 2D and E, unmodified F3.7, which contains the previously designated BRCA1 DNA binding domains (29–32), bound biotin-labeled, four-way junction-structured DNA (Fig. 2E, lane 2, top). Binding was DNA sequence–driven as opposed to biotin-driven, because excessive amounts of the same, unlabeled DNA blocked biotinyl DNA binding to F3.7, likely by competition (Fig. 2E, lane 5, top). However, when F3.7 was PARsylated by PARP1 (Fig. 2E, lanes 1, 4, and 7), its DNA binding activity was completely abolished (Fig. 2E, lane 1, top). Thus, PARsylation prevented BRCA1 F3.7 binding to a four-way DNA junction structure *ex vivo*.

Next, we modified the same system to test whether PARP1-driven BRCA1 PARsylation triggers the release of BRCA1 that is already bound to DNA (Fig. 2F). As shown in Fig. 2G, incubating biotinyl DNA–bound BRCA1 F3.7 (Fig. 2G, lane 2, bottom) with purified PARP1 and NAD completely released F3.7 from DNA (Fig. 2G, lane 3, bottom), and the released F3.7 was clearly PARsylated (Fig. 2G, lane 4, top). However, a significant amount of F3.7 remained DNA bound when PARP1 enzymatic activity was inhibited by olaparib (Fig. 2G, lane 5, bottom), and GST did not bind four-way junction-structured DNA (data not shown). Thus, PARsylation led to the release of BRCA1 F3.7 from a DNA substrate *in vitro*.

Stability of RAP80–BRCA1 Complexes after DNA Damage Requires BRCA1 PARsylation and Proper Interactions between Subunits

Because PARP1 is a RAP80–BRCA1 partner, we asked whether PARP1 enzymatic activity affects the integrity of RAP80–BRCA1 complexes. In cells exposed to a PARP inhibitor, olaparib, post-IR BRCA1–RAP80 binding was significantly weakened, particularly at late time points after irradiation (Fig. 3A, lanes 7–10). By contrast, olaparib exposure had no effect on the ability of CtIP, BACH1, or RAD51 to co-IP with BARD1, a heterodimeric partner of BRCA1 (ref. 38; Supplementary Fig. S6A), or on BRCA1–BARD1 co-IP (Fig. 3B, lanes 5–8).

In keeping with this observation, the interaction between the non-PARsylatable BRCA1 mutant BRCA1-D5 and RAP80 was mostly lost after DNA damage. However, its interaction with CtIP or BACH1 was unaffected (Supplementary Fig. S6B, compare lane 7 with lane 3). Thus, PARP1-driven BRCA1 PARsylation is required for stable BRCA1–RAP80 complex formation, but not for BRCA1–CtIP or BRCA1–BACH1 binding.

Just as olaparib disrupted the interaction between PARP1 and BARD1 (Fig. 3B, compare lanes 5–8 with lanes 1–4), *RAP80* depletion (by shRNA transduction) also disrupted the association between BARD1 and PARP1 (Fig. 3B, lanes 9–12). As expected, the interaction between BRCA1 and BARD1 was unaffected by either treatment (Fig. 3B, top). Thus, BRCA1 PARsylation and RAP80 are individually required for PARP1–BRCA1/BARD1–RAP80 complex stability.

Earlier studies showed that ABRA1 bridges RAP80 and BRCA1 and that the interaction between BRCA1 and ABRA1 does not require RAP80 either before or shortly after IR (i.e., ≤2 hours; refs. 10, 39, 40). However, at a late time point (4 hours) after IR, we found that ABRA1 binding to BRCA1/BARD1 was weakened in RAP80-depleted cells (Fig. 3B, lanes 9–12). Moreover, when cells were exposed to both *RAP80* shRNA and olaparib, the interaction between ABRA1 and BRCA1–BARD1 was further impaired (Fig. 3B, lanes 13–16).

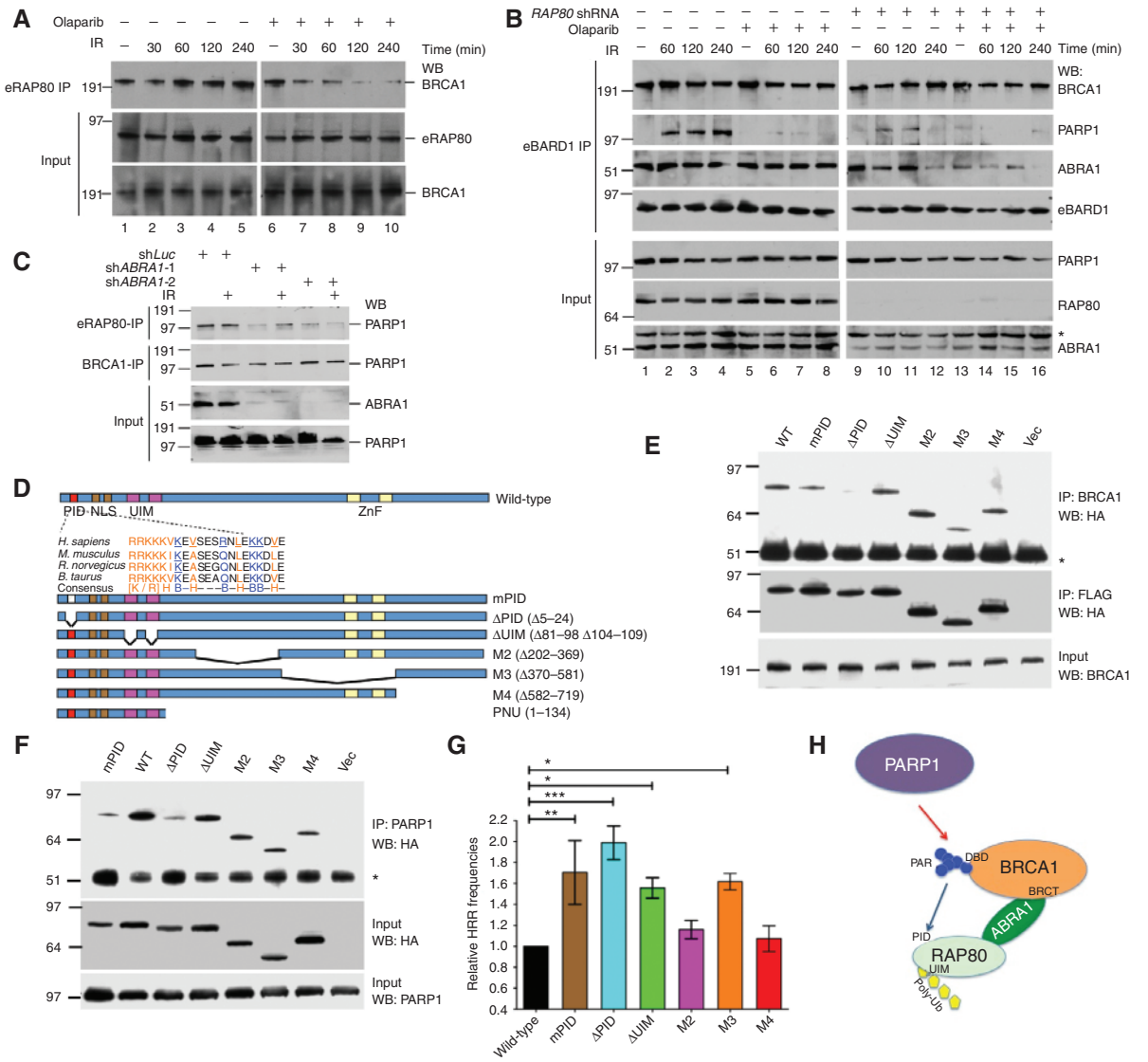

Figure 3. The interaction between PARsylated BRCA1 and RAP80 is required for maintaining BRCA1–RAP80–PARP1 complex integrity after DNA damage and normal HRR regulation. **A,** HeLa cells stably expressing FLAG/HA-tagged RAP80 (eRAP80) were incubated with 30 nmol/L olaparib for 48 hours and then irradiated with 10 Gy IR. Cells were lysed 30, 60, 120, or 240 minutes after IR. IPs were performed with antibodies directed against FLAG (recognizing eRAP80) and then probed with anti-BRCA1. Input samples were blotted and probed with an anti-HA (recognizing eRAP80) or an anti-BRCA1 antibody. **B,** HeLa cells that stably express FLAG/HA-tagged BARD1 (eBARD1) and an shRNA containing either a *RAP80*-targeting or a control sequence were generated. Where indicated, these cells were incubated with 30 nmol/L olaparib or DMSO for 48 hours. Cells were then irradiated with 10 Gy IR and lysed 60, 120, or 240 minutes later. IPs were performed with anti-FLAG antibody (recognizing eBARD1) and then probed with antibodies directed against BRCA1, PARP1, or ABRA1. Input proteins were blotted and probed with antibodies against PARP1, RAP80, or ABRA1. The asterisk in the ABRA1 blot indicates the migration position of a nonspecific band detectable by this antibody. **C,** HeLa cells stably expressing eRAP80 were infected with a lentivirus encoding an shRNA directed at Luciferase (sh*Luc*) or *ABRA1* (sh*ABRA1*-1 or sh*ABRA1*-2). Forty-eight hours later, cells were irradiated with 10 Gy IR or mock treated. Cells were collected 4 hours after IR. IPs were performed with antibodies directed at FLAG (recognizing eRAP80) or BRCA1 and then probed with anti-PARP1 antibody. Input samples were blotted and probed with an anti-ABRA1 or an anti-PARP1 antibody. **D,** RAP80 contains a PID. Schematic diagrams indicate the domain structure of human RAP80. ZnF, Zinc finger domain. The sequences of the PID domain in four mammalian species are shown. The conserved K/R-rich cluster, hydrophobic, and basic amino acids are indicated in different colors. Seven conserved amino acids (underlined) were mutated to alanine (A) in the mPID mutant. Structures of six N-terminal GST or C-terminal FLAG/HA-tagged RAP80 mutants and an N-terminal T7-tagged RAP80 PNU fragment are shown below. **E,** 293T cells were transiently transfected with the RAP80-FLAG/HA vectors described in **D** and, 72 hours later, cells were irradiated with 10 Gy IR. Cells were lysed 3 hours later, and IPs were generated with an anti-BRCA1 antibody; the immunoprecipitated proteins were blotted, and the blots were probed with an anti-HA (top and middle plots) antibody. *, the position of IgG heavy chain. Protein (15 μg) from each lysate was loaded onto each gel lane, and the subsequent blots were probed with an anti-BRCA1 antibody (bottom). **F,** 293T cells were treated as in **E**. IPs were performed with an anti-PARP1 antibody. Immunoprecipitated proteins were blotted and probed with an anti-HA antibody to recognize epitope-tagged RAP80 mutants (top). *, migration position of IgG heavy chain. Protein (15 μg) from each lysate was loaded onto each gel lane, and the subsequent blots were probed with anti-HA (middle) or anti-PARP1 antibody (bottom). **G,** a graph summarizing relative HRR frequencies of cells overexpressing WT RAP80 or various RAP80 mutants. DR-GFP HRR assays were performed as described in Methods. The abundance of GFP-positive (HRR) cells overexpressing WT RAP80 was normalized to one. Experiments were performed in triplicate, and error bars indicate SD. *, $P < 0.05$; **, $P < 0.01$; ***, $P < 0.001$. **H,** a schematic diagram showing the relationship between PARP1, BRCA1, ABRA1, and RAP80 in the HRR-tuning complex. Red arrow, PARP1 promotes BRCA1 PARsylation. Blue arrow, binding of PAR to the RAP80 PID domain. BRCA1–BRCT and DNA-binding (DBD) domains, and RAP80 UIM domain, are also indicated in the diagram.

Thus, RAP80 and PARsylation are also both required for stable BRCA1–ABRA1 interaction.

We then depleted ABRA1 from cells and examined its effects on RAP80–BRCA1/BARD1–PARP1 complex stability. Under this condition, the interaction between RAP80 and PARP1 was significantly weakened, but the interaction between BRCA1 and PARP1 was not affected (Fig. 3C). Thus, the association between RAP80 and PARP1, although indirect, is largely mediated through the BRCA1–ABRA1 complex.

These data reinforce the view that the overall integrity of RAP80–ABRA1–BRCA1/BARD1–PARP1 complexes is influenced by specific interactions between subunits, PAR, and PARsylated BRCA1. Parenthetically, because BRCA1 was still PARsylated in RAP80- or ABRA1-depleted cells (Supplementary Fig. S6C and data not shown), RAP80 and ABRA1 are not required for BRCA1 PARsylation *per se*.

Only a small fraction of the RAP80 within RAP80–BRCA1 complexes coimmunoprecipitated with PARsylated BRCA1 in an immunoprecipitation followed by re-immunoprecipitation (IP-re-IP) experiment (Supplementary Fig. S6D, lanes 5 and 6). This is in keeping with the knowledge that only a small fraction of BRCA1 in cells is PARsylated. Because rapid turnover is a common fate for DNA damage–induced ADP-ribose polymers (41), we speculate that BRCA1 PARsylation is a transient modification subject to rapid turnover.

RAP80 Possesses a Functioning PID That Is Required for Normal HRR Tuning

Some proteins that functionally communicate with PARP1 and/or PARsylated proteins contain specific domains that bind PAR. These PIDs play critical roles in performing and/or regulating PARsylation-related biologic processes (33, 42). One such PID contains a stretch of 19 to 21 amino acids that begins with a cluster of basic residues followed by a pattern of hydrophobic amino acids interspersed with basic residues (43–45). We identified such a 21-residue region at the N-terminus of RAP80. It is well conserved in mouse, rat, and bovine RAP80 (Fig. 3D).

To test whether this motif behaves as a *bona fide* PID, tagged RAP80 mutants were generated (Fig. 3D). The PAR-binding activity of purified GST-tagged, full-length WT RAP80 and of comparable amounts of these mutant derivatives (Supplementary Fig. S7A) was tested in a slot-blot binding assay. GST-WT RAP80 bound purified PAR polymers, whereas GST did not (Supplementary Fig. S7B). The PAR-binding capacity of mPID or ΔPID was significantly weaker than that of WT (Supplementary Fig. S7B), suggesting that RAP80 can bind PAR, mediated at least in part through its PID. Histone H1, which also contains a PID, served as a positive control (46).

We next asked whether the RAP80 PID could interact directly with PARsylated BRCA1. Because full-length RAP80 binds BRCA1 protein through multiple domains *in vitro* (data not shown), we tested the binding of a RAP80 fragment that retained only the PID, nuclear localization sequence (NLS), and ubiquitin-interacting motif (UIM) motifs (Fig. 3D, fragment PNU) to PARsylated and unmodified BRCA1 F3.7 (i.e., the BRCA1 segment targeted by PARsylation). Mutant fragments containing an mPID mutation, ΔPID, or a UIM deletion (ΔUIM) were also tested. The results indicate that the RAP80 PID but not its UIM domain is required for efficient binding to PARsylated BRCA1 F3.7. Moreover, PARsylation of BRCA1 F3.7 was required for this interaction (Supplementary Fig. S7C). Thus, the RAP80 PID facilitates the binding of PARsylated BRCA1 in the RAP80–BRCA1 complex.

Because PARsylation supports the integrity of RAP80–BRCA1 complexes after DNA damage (cf. Fig. 3A and Supplementary Fig. S6B), we asked whether the RAP80 PID contributes to this function. Consistent with the finding that the RAP80 PID is required for binding to PARsylated BRCA1 F3.7 *in vitro* (Supplementary Fig. S7C), HA-tagged mPID and ΔPID were defective in their association with intact BRCA1 in cells after IR by comparison with WT and other RAP80 mutants (Fig. 3E). Moreover, mPID or ΔPID was also defective in binding to endogenous PARP1 in cells (Fig. 3F). This implies that the PID is required for the stable association of RAP80 and PARP1 (through BRCA1; Fig. 3C). The interaction defect was not associated with failure of these mutants to concentrate in IRIF, because mPID and ΔPID concentrated there normally, whereas, as expected, ΔUIM failed to do so (refs. 8–10, 47; Supplementary Fig. S7D).

Thus, the RAP80 PID domain, likely through an interaction with PARsylated BRCA1, contributes to overall RAP80–BRCA1–PARP1 complex stability after DNA damage. That said, it is not required for RAP80 concentration in IRIF.

Because a defective PID cannot sustain a normal interaction between RAP80 and either BRCA1 or PARP1 (c.f. Fig. 3E and F), we asked whether expressing RAP80 mPID or ΔPID interferes with RAP80-driven HRR-regulation function. Indeed, expression of each resulted in significantly higher HRR frequencies in U2OS cells that contain a single, integrated DR-GFP HRR reporter (U2OS-DR-GFP; refs. 48, 49). As controls for nonspecific effects, two other deletion mutants that map outside of the PID sequence, M2 and M4, had no such effect (Fig. 3G). These data imply that RAP80–PAR binding is required to sustain proper HRR regulation.

ΔUIM expression also led to higher HRR frequencies. This result implies that RAP80–polyubiquitin binding, which tethers RAP80 in postdamage foci, is also required for it to function in HRR regulation (Fig. 3G).

ABRA1 serves as another bridge between RAP80 and BRCA1 (10, 39, 40). Thus, we wondered whether this interaction was also important for HRR regulation. The RAP80 sequences that are required for ABRA1 binding map to two partially overlapping regions within aa 235–400 of RAP80 (10, 39). Our RAP80 M2 and M3 mutants cover this region (Fig. 3D). Although the M3 mutant was functional for PAR binding *in vitro* (Supplementary Fig. S7B), its binding to BRCA1 was considerably weaker than WT (Fig. 3E), presumably due to its defective interaction with ABRA1. Consistent with this observation, expression of the M3 mutant also resulted in increased HRR (Fig. 3G).

Therefore, in addition to maintaining the integrity of RAP80–ABRA1–BRCA1/BARD1–PARP1 complexes, these results imply that the contribution to HRR regulation by RAP80 also requires its intact PID–BRCA1 and ABRA1–BRCA1 interactions as well as normal UIM-polyubiquitin binding (Fig. 3H).

BRCA1 PARsylation Is Required for Normal HRR Regulation

Consistent with the observation that olaparib led to increased BRCA1 chromatin association at sites near a single

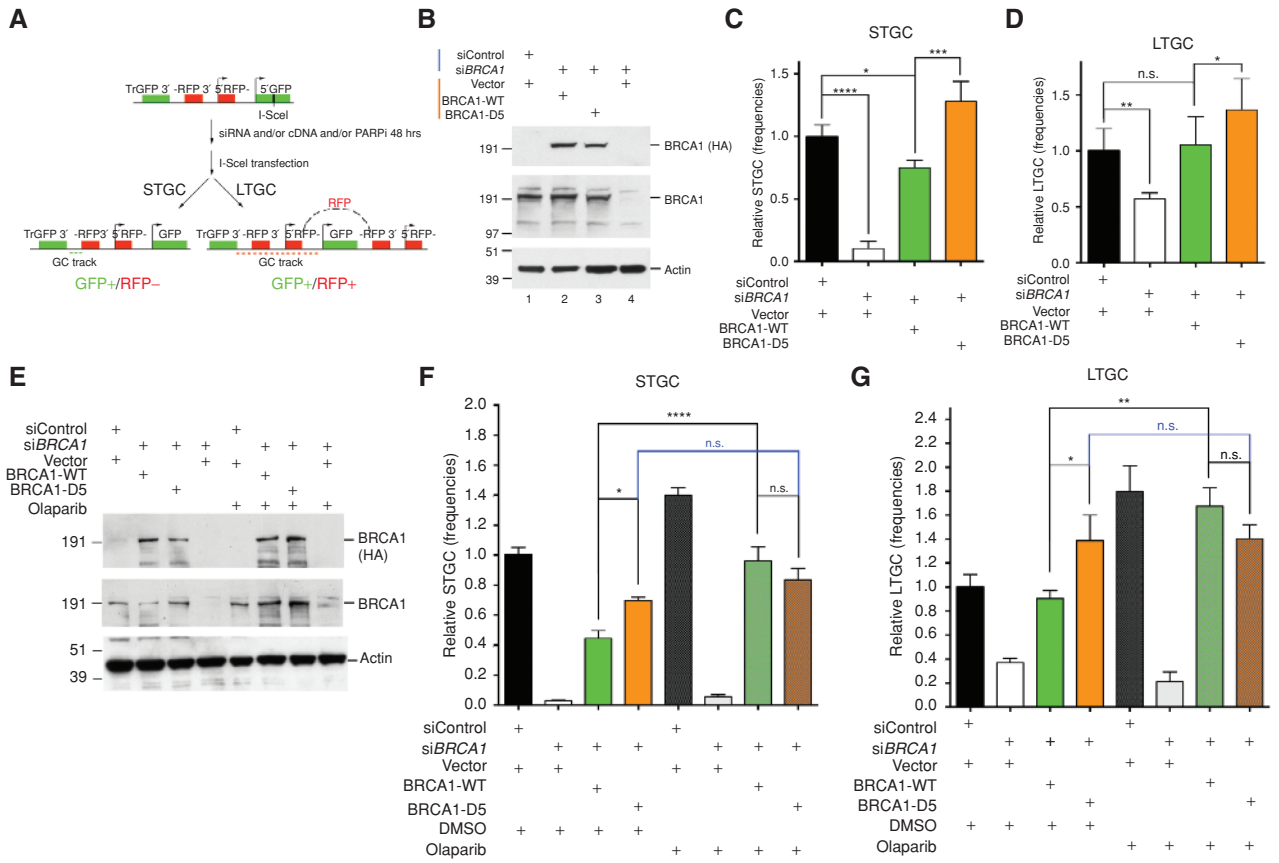

Figure 4. BRCA1 PARsylation is required for normal HRR tuning. **A,** a schematic diagram showing the steps in the I-*Sce*I–induced DSB HR repair assay, using cells containing a single copy of the SCR reporter that can measure both short track gene conversion (STGC) and long track gene conversion (LTGC). Tr-GFP: a 5′ truncated GFP fragment; -RFP3′: 3′ exon of the RFP cassette; 5′RFP-: 5′ exon of the RFP cassette; 5′GFP: a 3′ truncated GFP cassette containing the I-SceI recognition sequence. STGC results in a smaller gene conversion track (green dashed line) and only restores the GFP cassette. LTGC results in a longer gene conversion track and duplications (red dashed line) that lead to a functional RFP cassette by restoring the correct order of RFP exons (black dashed line above the GFP cassette on the right). **B–D,** effects of BRCA1-WT and BRCA1-D5 on STGC and LTGC. U2OS cells containing the SCR reporter were sequentially transfected with *BRCA1* siRNA and siRNA-resistant BRCA1-WT or BRCA1-D5. STGC and LTGC assays were performed as described in Methods. **B,** Western blots showing depletion of endogenous BRCA1 and expression of BRCA1-WT or BRCA1-D5 in these reporter-containing cells. Protein (25 μg) was loaded in each lane, and the blot was probed with antibodies directed against HA (detects HA-tagged BRCA1-WT or BRCA1-D5), BRCA1, or actin. **C,** results of STGC assay. The STGC frequencies of cells transfected with control siRNA plus vector were normalized to one. **D,** results of LTGC assay. The LTGC frequencies of cells transfected with control siRNA and vector were normalized to one. **E–G,** effects of olaparib on STGC and LTGC in cells depleted of BRCA1 or expressing endogenous BRCA1, or depleted of endogenous BRCA1 and expressing ectopic BRCA1-WT or BRCA1-D5. **E,** Western blots showing depletion of endogenous BRCA1 and reexpression of BRCA1-WT or BRCA1-D5 in cells. These cells were either treated with DMSO or 30 nmol/L olaparib for 48 hours before being transfected with an I-*Sce*I–expressing plasmid. Protein (25 μg) was loaded in each lane, and the blot was probed with HA (detects HA-tagged BRCA1-WT or BRCA1-D5), BRCA1, or actin antibodies. **F,** results of STGC assay. The STGC frequencies of cells transfected with control siRNA and vector were normalized to one. **G,** results of LTGC assay. The LTGC frequencies of cells transfected with control siRNA and vector were normalized to one. *, $P < 0.05$; **, $P < 0.01$; ***, $P < 0.001$; ****, $P < 0.0001$; n.s., not significant.

DSB (Supplementary Fig. S5), the magnitude of HR repair of this DSB increased after PARP1 depletion or exposure to 30 nmol/L olaparib (Supplementary Fig. S8A–S8C). A similar increase was observed in a mouse embryonic stem (ES) cell line containing an independent HRR reporter (Supplementary Fig. S8D). At this olaparib concentration, the inhibitor blocked PARP1 enzymatic activity effectively but did not cause detectable DNA damage, cell-cycle changes, or toxicity (Supplementary Fig. S8E and S8F).

Two studies previously reported that PARP1 inactivation or inhibition did not affect the outcomes of I-*Sce*I–induced HRR (50, 51). To address the apparent difference in our observations, we compared the effects of four different PARP inhibitors—1,5-dihydroxyisoquinoline (ISQ), which was used in one of the two studies noted above (50), olaparib, veliparib, and BMN-673. BMN-673 is the most potent and specific PARP1 inhibitor known to date with an IC_{50} against PARP1 of approximately 0.5 nmol/L (52). In this experiment, we used a U2OS cell line that allows one to measure both I-*Sce*I–induced short track gene conversion (STGC)–type and long track gene conversion (LTGC)–type HRR (Fig. 4A). The former is a faithful reflection of error-free HRR, and the latter could give rise to nonallelic, error-prone recombination events (53, 54).

When cells were exposed to each of these inhibitors over a range of relatively low concentrations (i.e., 5–40 times the IC_{50} for PARP1 for each inhibitor; Supplementary Fig. S8G), all four stimulated HRR (both STGC and LTGC) to various extents (Supplementary Fig. S8H and S8I). However, at

higher doses, ISQ either had no effect (at 75 μmol/L) or actually inhibited HRR (at 300 μmol/L; Supplementary Fig. S8H and S8I). The ISQ concentration used in the earlier report was 600 μmol/L (50). These data suggest the presence of an off-target effect by a compound (ISQ) with significantly lower avidity for PARP1 than the other inhibitors. Thus, the effect of PARP inhibitors on HRR is dose dependent. Within a range that elicited what are likely to be on-target effects, HRR stimulation was a constant finding.

To further determine the effect of BRCA1 PARsylation on HRR and to avoid potential confounding effects of PARP1 inhibition or depletion, we analyzed cells that transiently expressed HA-tagged BRCA1-WT or identically tagged, PARsylation-defective BRCA1-D5. Each was expressed at levels comparable to that of endogenous BRCA1. Moreover, the mRNA for both had been rendered *BRCA1* sh/siRNA resistant. Expression of endogenous BRCA1 was suppressed by shRNA and siRNA, respectively, followed by a comparison of the frequencies of HR-mediated repair of a single I-*Sce*I–induced DSB in these cells and controls (Fig. 4B).

Surprisingly, RNAi-resistant BRCA1-D5 expression in BRCA1-depleted cells led to significantly higher HRR frequencies (for both STGC and LTGC) than those observed in both control cells and cells reexpressing BRCA1-WT (Fig. 4C and D, compare column 3 and 4). In addition, olaparib treatment led to an enhancement of both STGC and LTGC in cells expressing BRCA1-WT, but not in cells expressing BRCA1-D5 (Fig. 4E–G). This implies that the observed HRR stimulation caused by olaparib within its on-target concentration range is mostly contributed by a failure of proper BRCA1 PARsylation.

These data indicate that BRCA1 PARsylation is required for normal HRR amplitude regulation. We hypothesize that the hyper-HRR phenotype associated with PARP1 inhibition is a product of defective BRCA1 PARsylation, because it was the only major difference observed between BRCA1-D5 and BRCA1-WT–driven HHR function in these experiments.

BRCA1 PARsylation Is Required for Maintaining Chromosome Integrity in Response to DNA Damage

Recent studies demonstrated that the chromosomal rearrangements observed after IR exposure in BRCA1-deficient cells are largely a product of combining inactive HRR with overactive, end joining–mediated, and erroneous repair of DSBs (55, 56). Because cells in which endogenous, WT BRCA1 was replaced by the non-PARsylatable mutant BRCA1-D5 actually revealed higher HRR activity (cf. Fig. 4C and D), we asked whether there were fewer rearranged chromosomes induced by DNA damage in these cells compared with cells expressing comparable amounts of BRCA1-WT (Supplementary Fig. S9A).

To test this possibility, we irradiated cells and then analyzed them for chromosomal abnormalities. Each damaged or rearranged chromosome present in a series of cell spreads was assigned to one of four categories: (i) fusions/bridges (F), in which two chromatids from different chromosomes appear to be connected; (ii) radial structures (R), in which chromosomes are composed of three- or four-armed structures; (iii) complex rearrangements (C), in which three or more chromosomes are connected to form complex structures that cannot be assigned to any of the other three types; and (iv) chromatid breaks/gaps (B; Fig. 5A).

Compared with cells transduced with control (sh*Luc*) shRNA, cells in which endogenous BRCA1 was depleted by sh*BRCA1* (Supplementary Fig. S9A) displayed significantly higher frequencies of fusions/bridges (Fig. 5B, column 2) and radial structures (Fig. 5C, column 2). But there were only slight increases in complex rearrangements (Fig. 5D, column 2) and breaks/gaps (Fig. 5E, column 2) in these cells.

Reintroduction of shRNA-resistant BRCA1-WT expression in these endogenous BRCA1-depleted cells (Supplementary Fig. S9A) partially reduced the frequencies of fusion/bridges (Fig. 5B, column 3) and radial structures (Fig. 5C, column 3).

As described earlier, cells reconstituted with the non-PARsylatable BRCA1-D5 revealed a higher HRR amplitude than those reconstituted with BRCA1-WT (cf. Fig. 4C and D). Thus, we expected to find that BRCA1-D5–expressing cells revealed even fewer damaged chromosomes than BRCA1-WT–reconstituted expressing cells. Surprisingly, BRCA1-D5–expressing cells revealed significantly higher frequencies of fusion/bridges (Fig. 5B, column 4), radial structures (Fig. 5C, column 4), and complex rearrangements (Fig. 5D, column 4) than those of cells expressing BRCA1-WT. Indeed, the frequencies of complex rearrangements in BRCA1-D5–expressing cells were 5- to 7-fold higher than those in control, BRCA1-depleted cells either before or after BRCA1-WT reexpression (Fig. 5D, compare column 4 with columns 1, 2, and 3). In contrast, there was no difference in the frequencies of breaks/gaps between BRCA1-WT and BRCA1-D5 reexpressing cells (Fig. 5E, column 4).

Given these observations, we hypothesized that certain forms of chromosome rearrangement observed in cells expressing BRCA1-D5 might be the result of aberrant HRR-dependent repair. To test this, we cotransfected cells with siRNAs targeting *RAD51* or *EXO1+DNA2L*. RAD51 is the prime recombinase required for performing homology search and strand exchange reactions in HRR (57). EXO1 and DNA2L are two major nucleases that facilitate the generation of long, single-stranded DNA segments needed for HRR (58).

Importantly, depletion of either RAD51 or EXO1+DNA2L reduced the levels of both radial structures (Fig. 5C, compare columns 7 and 10 with column 4) and complex rearrangements (Fig. 5D, compare columns 7 and 10 with column 4) in BRCA1-D5–expressing cells. This suggests that these two types of chromosome aberration in cells expressing BRCA1-D5 were dependent upon key aspects of the HRR mechanism.

Transfecting cells with *RAD51* or *EXO1+DNA2L* siRNAs resulted in the blocking of HRR downstream of BRCA1–CtIP (59, 60). This would result in arrested repair of those initial IR-induced chromosomal breaks that would have been repaired by HRR. Therefore, we expected to observe higher accumulations of chromosomal breaks/gaps in cells expressing BRCA1-D5 than in control, BRCA1-depleted, or BRCA1-WT reexpressing cells, when *RAD51* or *EXO1+DNA2L* were depleted. This was indeed the case (Fig. 5E, columns 7 and 10). This result further suggests that hyperactive, aberrant HRR is responsible for the radial structures and complex rearrangements seen in cells expressing BRCA1-D5.

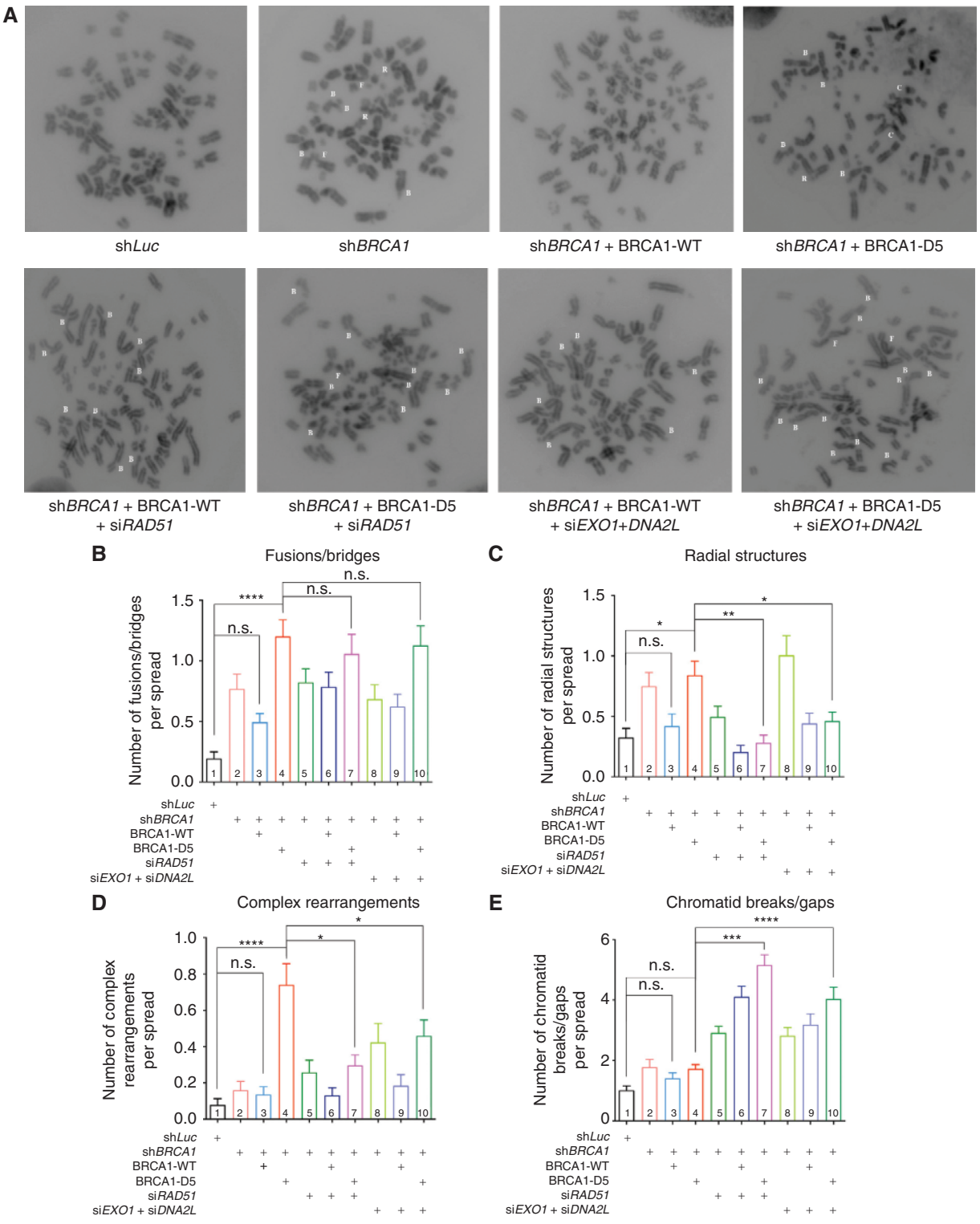

Figure 5. Defective BRCA1 PARsylation results in HRR-dependent chromosome rearrangements after IR. **A,** representative metaphase spreads of U2OS cells: transduced with control shRNA (sh*Luc*), sh*BRCA1*, transduced with sh*BRCA1* and re-expressing BRCA1-WT or BRCA1-D5, or cells transfected with *RAD51* siRNA or *EXO1+DNA2L* siRNA in addition to the previous treatment. Cells were irradiated with 150 rad and collected 8 hours later for chromosome analysis. White letters in each spread indicate the nature of aberrant chromosomes present: B, chromatid breaks/gaps; F, fusions/bridges; R, radial structures; C, complex rearrangements. **B–E,** bar graphs showing frequencies of these various aberrant chromosomes in cells treated with indicated combinations of shRNA, siRNA, and/or cDNAs. **B,** frequencies of fusions/bridges. **C,** frequencies of radial structures. **D,** frequencies of complex rearrangements. **E,** frequencies of chromatid breaks/gaps. At least 50 metaphase spreads were counted for each category of cells. Statistical analyses were performed using the Kruskal–Wallis tests. Results of selected multiple comparisons are shown. *, $P < 0.05$; **, $P < 0.01$; ***, $P < 0.001$; ****, $P < 0.0001$; n.s., not significant.

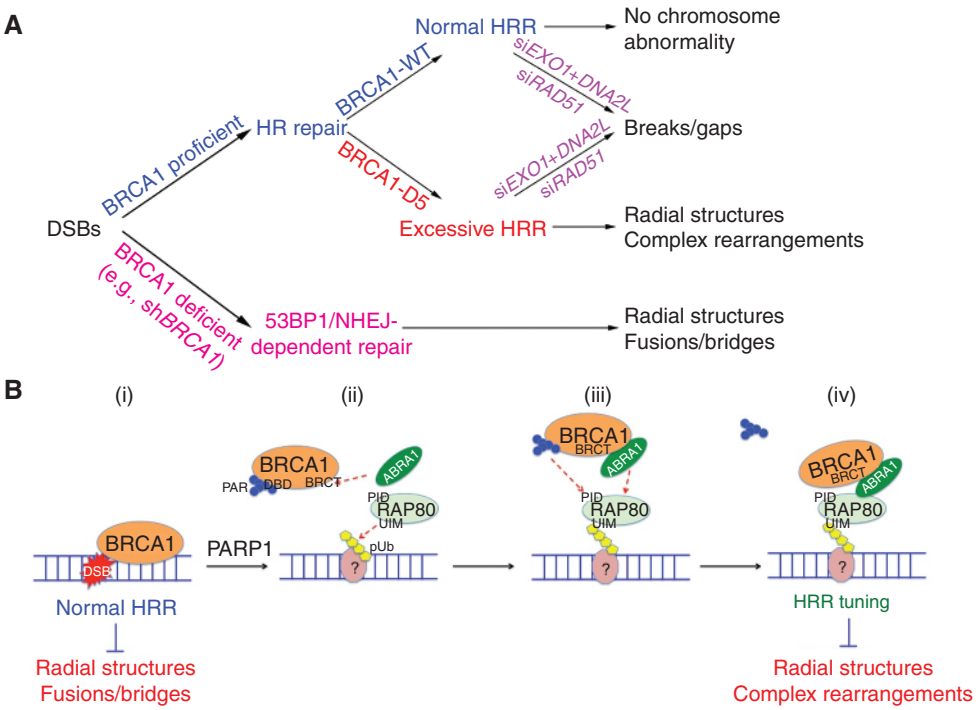

Figure 6. Models showing the effects of BRCA1 PARsylation on genome integrity control after DNA damage. **A,** a schematic diagram showing the development of nonhomologous end joining (NHEJ)–dependent or HRR-dependent chromosome damage and rearrangements in cells depleted of BRCA1 or in cells expressing either wild-type BRCA1 (BRCA1-WT) or non-PARsylatable BRCA1 (BRCA1-D5), respectively. **B,** a schematic diagram showing the role of timely PARP1-driven BRCA1 PARsylation in HRR tuning and genome integrity control. i, BRCA1 normally promotes HRR by interacting with damaged DNA and recombination intermediates. Normal HRR suppresses the development of radial structures and fusions/bridges. ii, PARP1-driven BRCA1 PARsylation releases BRCA1 from DNA by targeting its DNA binding domain (DBD). ABRA1 interacts with BRCA1–BRCT domain, and RAP80 binds to polyubiquitin chains (pUb) formed at or near the site of DNA damage (indicated by a circle with "?" because the nature of the chromatin structure involved remains unclear). The sequence of these events is unknown, and it is possible that they occur concurrently. iii, RAP80 interacts with PARsylated BRCA1 through its PID and also through its interaction with ABRA1. iv, PAR is removed after the formation of stable RAP80–ABRA1–BRCA1 complexes. The successful completion of these steps ensures proper HRR amplitude control (i.e., tuning) and prevents the development of radial structures and complex chromosome rearrangements.

In these experiments, RAD51 depletion elicited a much stronger inhibitory effect on HRR than EXO1+DNA2L depletion, because other nucleases could compensate for some lost function of EXO1 and DNA2L (Supplementary Fig. S9B). Moreover, RAD51 function is considered essential for HRR. This may help to explain why RAD51 depletion led to a more extensive reduction in radial structures and complex rearrangements than depletion of EXO1+DNA2L (Fig. 5C and D).

In summary, these observations indicate that defective BRCA1 PARsylation, observed in cells expressing BRCA1-D5 in place of WT BRCA1, fosters the development of chromosome aberrations after DNA damage. Thus, loss of BRCA1 function, which leads to HRR deficiency and a preference for nonhomologous end joining (NHEJ)–type repair, and deregulated, excessive BRCA1 HRR activity can both elicit deleterious, mutagenic chromosome instability (Fig. 6A and B).

Finally, RAD51 or EXO1+DNA2L depletion had no significant impact on the frequencies of fusions/bridges in cells expressing BRCA1-D5, which remained significantly higher than other groups of cells (Fig. 5B). We speculate that a BRCA1-D5 function other than promoting hyper-HRR is responsible for this abnormal phenotype. This is consistent with the fact that BRCA1 engages in repair processes other than HRR and that BRCA1-D5 may participate in these and yet other deregulated repair processes (61, 62)

The BRCA1 PARsylation–RAP80 Pathway Is Defective in a Subset of Breast Cancer Cells and Tumors

Because *BRCA1* is a breast cancer gene, we investigated whether BRCA1 is PARsylated in normal human mammary and breast cancer cells. Here, we examined a panel of 13 well-established sporadic breast cancer cell lines along with iMECs, a telomerase-immortalized normal, primary mammary epithelial cell line (Fig. 7A). Among the 13 breast cancer cell lines, 9 were characterized as triple-negative, basal-like (TNBC, i.e., ER^-, PR^-, and *HER2* not amplified) subtype. Two of them contained disease-producing mutations in the *BRCA1* gene. The remaining four were of the luminal subtype (63, 64).

We evaluated the status of BRCA1 PARsylation in these cell lines before and after IR by IP–Western assay (Fig. 7A). Surprisingly, although comparable levels of intact BRCA1 p220 were detected in all but the two *BRCA1*-mutant lines (HCC1937 and SUM149; Fig. 7A), the levels of PARsylated BRCA1 were significantly lower or even undetectable in

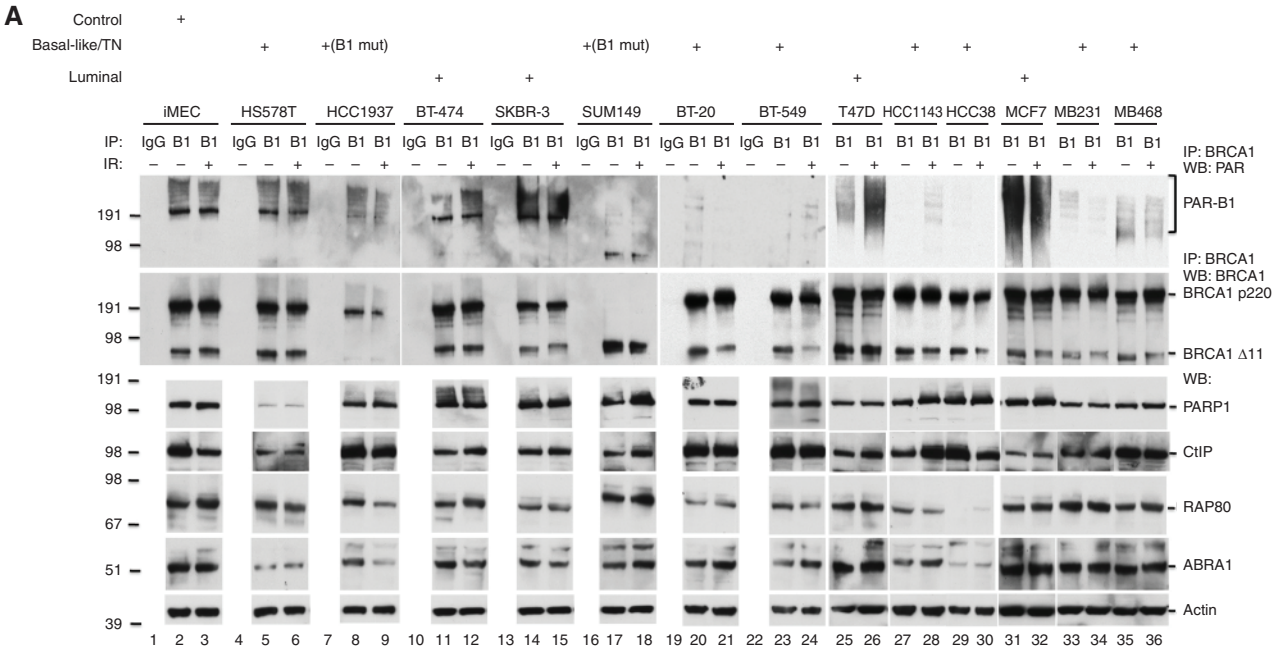

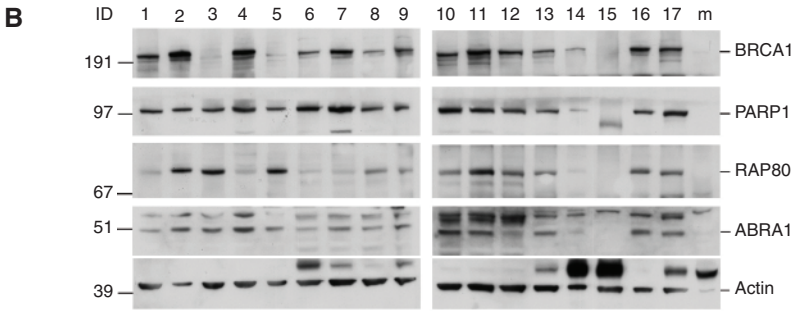

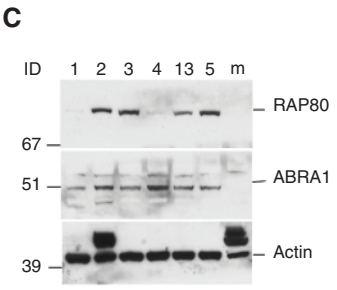

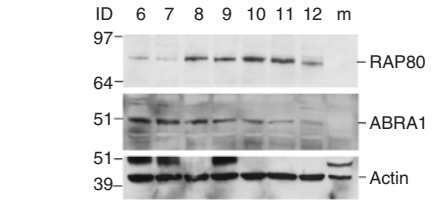

E

Patient ID	Subtype	BRCA1	RAP80	ABRA1	BRCC36	PARP1	BRCA2	RAD51
1	ER+	+	–	+/–	+	+	–	+
2	TNBC	+	+	+	+	+	–	+
3	TNBC	–	+	+	+	+	+	+
4	ER+	+	–	+	+	+	+	+
5	ER+	–	+	+	+	+	+	+
6	TNBC	+	–	+	–	+	+	+
7	TNBC	+	–	+	+	+	+	+
8	HER2+	+/–	+/–	+	+	+	–	+
9	ER+	+	+/–	+	+	+	+	+
10	TNBC	+	+	+	+	+	+	+
11	TNBC	+	+	+	+	+	+	+
12	TNBC	+	+	+/–	+	+	+	+
13	TNBC	+	+	+	+	+	+	+
14	HER2+	+/–	–	–	N.D.	+/–	N.D.	N.D.
15	TNBC	–	–	–	N.D.	–	N.D.	N.D.
16	TNBC	+	+	+	N.D.	+	N.D.	N.D.
17	TNBC	+	+	+	+	+	+	+

Figure 7. BRCA1 PARsylation and/or RAP80 expression is suppressed in a subset of breast cancer cell lines and tumors. **A,** results of IP–Western blots searching for BRCA1 PARsylation in a panel of normal breast and breast cancer cell lines (the pathologic subtype of each cell line is indicated above the relevant blot; B1 mut, cell lines that contain pathologic *BRCA1* mutations). Cells were irradiated with 10 Gy IR or mock treated, and collected 8 hours later for analysis. IPs were performed using a rabbit polyclonal anti-BRCA1 antibody. Immunoprecipitated proteins were blotted and probed with a monoclonal anti-PAR antibody (top plots) or a monoclonal anti-BRCA1 antibody (the second row of plots). Protein extract (20 μg) from each cell line was blotted and probed with antibodies recognizing PARP1, CtIP, RAP80, ABRA1, and actin, respectively. **B–D,** results of Western blots detecting BRCA1, PARP1, RAP80, ABRA1, and actin expression in subsets of tumor samples from PDX models. Protein extract (20 μg) from each tumor was blotted and probed with antibodies recognizing the above noted proteins. "m" indicates lanes that were loaded with extracts from mouse breast tissues. Please note that mouse BRCA1, RAP80, and ABRA1 were not detectable by the antibodies used, which specifically recognize human proteins. Results shown were obtained in three different experiments using independent snap-frozen tumor samples (see Supplementary Methods). **E,** table summarizing the results of protein expression analysis by Western blotting of tumor samples from 17 PDX models. +, positive; –, negative; +/–, weaker expression than other samples. Samples with defective RAP80 and/or ABRA1 expression are indicated in red. N.D., not determined.

6 lines, all of which were derived from sporadic TNBC (Fig. 7A, top). This suggests the existence of certain defects in the generation and/or maintenance of BRCA1 PARsylation in a subset of breast cancer lines that express WT BRCA1.

We next asked whether similar defects in BRCA1 PARsylation and/or RAP80 expression are also present in primary human breast tumors. However, because the only way to detect BRCA1 PARsylation is IP–Western blotting, which requires large amounts of freshly prepared protein lysates, we were unable to obtain results of satisfactory quality from primary tumor samples.

Therefore, we turned to an analysis of patient-derived xenograft (PDX) breast cancer tumors, which have been shown to resemble, pathologically and genetically, the primary tumors from which they were derived (65–67). Although the status of BRCA1 PARsylation remained undetermined due to high background signals (likely from host mouse tissues), we repeatedly detected defects in RAP80 and/or ABRA1 expression in some of these tumors (Fig. 7B–D). A summary of these observations is provided in Fig. 7E.

DISCUSSION

We have identified PARP1 as a physiologic partner of the RAP80–BRCA1 complex. PARP1 PARsylates BRCA1, a pivotal contributor to HR-mediated DSB repair. Although PARP1-driven BRCA1 PARsylation is not required for HRR function *per se*, it represents a critical step in its regulation (aka tuning). BRCA1 PARsylation is targeted to a polypeptide segment within its DNA binding domain and is controlled by a short oligopeptide sequence, D5, that resides near the center of this segment. PARsylation modulates BRCA1 DNA binding activity *in vitro* and is required for normal HRR tuning. It is required to suppress the development of a hyper-HRR state. Importantly, following DNA damage, hyper-recombination resulting from defective BRCA1 PARsylation constitutes a genome-destabilizing force (Fig. 6B).

The function of BRCA1 in supporting HRR has long been considered an important suppressor of breast and ovarian cancers (2). This notion was strengthened by the observation that chromosome instability and cancer development arising when BRCA1 function is absent from cells are mainly the result of an inability to activate normal DSB end-processing by BRCA1 and/or by certain of its partner proteins that are required for HRR (55, 56).

However, recent observations indicate that excessive BRCA1 activity and/or failure to regulate such activity is also associated with genomic instability (12, 13, 68). Importantly, as shown here, BRCA1 PARsylation, which requires a built-in, *cis*-acting BRCA1 element (i.e., D5), contributes to the BRCA1 genome integrity control system. Given the strong connection between its genome integrity control and its tumor suppression function, it is likely that D5 function contributes to BRCA1 tumor–suppressing activity.

The exact action by the D5 sequence that results in the licensing of BRCA1 PARsylation remains unknown. The D5 sequence is not the direct target of PAR coupling (Supplementary Fig. S3), and its integrity is not required for the DNA binding activity of full-length BRCA1 in the absence of PARsylation (data not shown). A mutant D5 sequence also failed to interfere with BRCA1 recruitment to sites of DNA damage (i.e., nuclear foci) or its interactions with known BRCA1 partner proteins that perform important steps in HRR (cf. Supplementary Figs. S4 and S6). Therefore, it is possible that the role of this sequence is to maintain a critical structural conformation of BRCA1 that is required for proper and timely PARsylation and subsequent modulation of BRCA1 DNA binding activity. Yet other possibilities exist. However, due to the location of the D5 sequence within the exon 11-encoded region, which is neither functionally nor structurally well characterized, we are currently unable to test the conformation hypothesis.

Unexpectedly, hyper-recombination resulting from defects in BRCA1 PARsylation was associated with the appearance of radial structures and complex chromosome rearrangements shortly after DNA damage. In contrast to the radial structures observed in BRCA1-depleted cells, which are dependent on 53BP1 and the NHEJ pathway (55, 56), those observed in BRCA1-D5–expressing cells were hyper-HRR dependent. The complex rearrangements observed in BRCA1-D5 cells were similarly hyper-HRR dependent (cf. Figs. 5 and 6A). Because these rearranged chromosomes emerged within one cell cycle, they might represent products of unresolved recombination intermediates.

PARP1 is an abundant enzyme that likely participates in multiple pathways, which, directly or indirectly, affect the outcome of HRR. Two previous reports, both of which also used I-*Sce*I–based HRR reporters, concluded that PARP1 is not involved in the repair of I-*Sce*I–induced DSBs (50, 51)—in contrast to what was reported here. In keeping with the apparent off-target effects triggered by very high concentrations of ISQ (cf. Supplementary Fig. S8G–S8I), differences in experimental conditions may have contributed to this discrepancy. In addition, the immortalized *Parp1*$^{-/-}$ MEF cells used in one of the above-noted studies (51) retained detectable, albeit low-level BRCA1 PARsylation activity, probably due to compensatory effects of other PARP enzymes (ref. 21; Fig. 1F). Therefore, a possible explanation for the lack of effect on HRR in these *Parp1*$^{-/-}$ MEFs is that other PARPs, through an emerging state of adaptation, were able to support normal HRR regulation at a single I-*Sce*I–induced DSB in these cells. Whatever the case, the demonstration that ISQ, at concentrations much closer to its IC_{50}, enhanced HRR, much like three more specific PARP inhibitors (Supplementary Fig. S8H and S8I), reinforces the view that PARP1 functions, at least in part, by negatively regulating BRCA1-driven HRR function.

Thus, we speculate that preventing the formation of proper RAP80–BRCA1–PARP1 complexes and blocking BRCA1 PARsylation, e.g., with a suitable PARP1-inhibiting agent or by replacing endogenous BRCA1 with a non-PARsylatable mutant, will translate into a major breakdown in HRR control. Because HRR control is also a suppressor of radial and complex chromosomal rearrangements, this effect is likely to be accompanied by overt chromosomal instability (Fig. 6). Such an outcome would be expected in any proliferating cell, such as certain hematopoietic progenitor cells in the bone marrow. Sufficient chronic genome disorder could, in time, nurture elements of a neoplastic phenotype.

Multiple PARP inhibitors are being tested in clinical trials as a novel class of therapeutic agents. BRCA1- or BRCA2-deficient

cancer cells are hypersensitive to PARP inhibitors due to their inability to repair PARP inhibitor–induced DNA damage or trapped PARP–DNA complexes in the absence of efficient HRR (69–72). Currently, PARP inhibitors are under clinical investigation for use in other cancers that synthesize fully functional BRCA1, such as ovarian cancers, either as a single agent or in combination with other therapeutic agents (73, 74). However, our results suggest that the use of PARP inhibitors in a BRCA1-proficient background requires caution, because chronic hyper-recombination in conjunction with sporadic or therapeutic DNA damage may result in deleterious genomic instability in nontumor cells.

Given the value of HRR tuning in genome stability control, one wonders whether it also operates in breast cancer suppression, because BRCA1 PARsylation defects were noted in some sporadic TNBC cell lines (Fig. 7A). If so, PARP1+RAP80-driven regulation of the amplitude of BRCA1 HRR function would be a physiologic process that, if defective, might be clinically relevant.

Recent studies suggest that certain mutations or polymorphisms in the *RAP80, ABRA1,* or *MERIT40/NBA1* (another member of the RAP80 complex) genes are associated with increased susceptibility to breast and/or ovarian cancer (75–80). In addition, the genomic region containing the RAP80 gene is not infrequently lost in TNBCs, which commonly exhibit gross manifestations of genomic instability (81). RAP80 and/or ABRA1 expression was also suppressed in 6 of 17 of our PDX breast cancer models, of which 3 were TNBCs in origin (Fig. 7E). Finally, cells of RAP80 or ABRA1 knockout mice experience a breakdown in genome integrity control, and these mice are more cancer prone than WT controls (82–84). These observations, together with our findings, suggest that a deficiency in RAP80 complex function and/or BRCA1 PARsylation contributes to the genomic instability that drives cancer development.

METHODS

For additional Methods, please see Supplementary Information.

Cell Culture

All cells were cultivated at 37°C in a humidified incubator in an atmosphere containing 10% CO_2. U2OS, HeLa, 293T, T98G, and MEF cells were grown in DMEM supplemented with 10% FBS. HeLa S3 cells were grown in Joklik's Minimum Essential Medium (Sigma) supplemented with 7% newborn calf serum at 37°C. Mouse ES cells were grown in ES medium (Invitrogen) on either MEF feeder cells or gelatinized plates supplemented with leukemia inhibitory factor (LIF), and cultured at 37°C in a humidified incubator in an atmosphere containing 5% CO_2. iMEC cells were grown in MEBM medium (Lonza Walkersville) supplemented with mammalian epithelium growth factors. Breast cancer cell lines were cultured according to the guidelines provided by the ATCC or the suppliers. No authentication of these cell lines was performed by the authors.

I-SceI Recombination Assay

U2OS cells containing a single copy of the DR-GFP reporter (U2OS-DR) were employed using methods that were described previously (49). Experiments using U2OS or mouse ES cell lines, each containing a single copy of the sister chromatid recombination (SCR) reporter, were performed as described (85). Two versions of the SCR reporter were used in experiments. One detects LTGC events by forming blasticidin (BSD)-resistant colonies, whereas the other measures LTGC events by counting cells with red fluorescent protein (RFP) fluorescence. Briefly, for the STGC assay, cells were transfected with pCBASce (I-*Sce*I) plasmid and collected 72 hours later. GFP-positive cell populations (i.e., STGC) were detected and measured by flow cytometry. For the LTGC assay, after pCBASce transfection, cells were either plated in 60-mm plates at 5×10^5 cell per plate and then selected with 10 μg/mL BSD beginning 48 hours later for 12 days, or measured by flow cytometry for RFP-positive cells. In all experiments, a plasmid expressing DsRed was transfected in parallel to determine transfection efficiency. To determine plating efficiency, cells were plated in 60-mm plates at 5,000 cells/plate but were not selected with BSD. In the case of BRCA1-depleted and BRCA1-reconstituted cells, because their ability to form colonies was compromised, the rates of cell survival after BSD selection were determined using the CellTiter-Glo method (Promega) following the manufacturer's protocol.

PARG Treatment

Immunoprecipitated proteins were eluted by incubating beads with elution buffer (0.1 mol/L Glycine, pH 2.5, 0.1 mol/L NaCl). The eluted protein-containing solution was diluted with 2× PARG reaction buffer (100 mmol/L KH_2PO_4, 100 mmol/L KCl, 0.2 mg/mL BSA, 0.2% Triton X-100). Recombinant PARG (Trevigen) was added to a final concentration of 10 ng/mL, and the reaction mixture was incubated at room temperature for 60 minutes.

PARP Inhibitor

The PARP inhibitors olaparib (AZD2281), veliparib (ABT-888), ISQ, and BMN-673 were dissolved in DMSO and stored at −20°C. When used in tissue culture experiments, each was further diluted in tissue culture medium. In most experiments, the final concentration of olaparib in the medium was 30 nmol/L, and control cells were incubated with medium containing the same concentration of the solvent, DMSO (final concentration: 0.003%).

Biotinylated-NAD Incorporation

HeLa cells growing in plates were washed twice with PBS and then incubated with PARP reaction buffer [56 mmol/L HEPES, pH = 8.0, 28 mmol/L KCl, 2 mmol/L MgCl2, 0.01% digitonin, 12.5 μmol/L biotinylated-NAD (Trevigen), supplemented with 100 nmol/L olaparib or 0.01% DMSO] for 30 minutes at 37°C. Cells were then collected and lysed in preheated denaturing lysis buffer [400 mmol/L NaCl, 0.5 mmol/L EDTA, 50 mmol/L Tris-HCl, pH 7.5, 0.5% NP-40, 70 mmol/L β-Mercaptoethanol, 1.5 mmol/L MgCl2, 10% glycerol, 5 mmol/L N-Ethylmaleimide (NEM), 1 μmol/L ADP-HPD (a PARG inhibitor) and protease inhibitors] and heated for 10 minutes at 95°C. After incubating for 30 minutes at 4°C, lysates were cleared by centrifugation and then incubated with Streptavidin M-280 Dynal beads (Invitrogen) to trap Biotin-containing proteins according to the manufacturer's guidelines.

In Vitro *ADP-Ribosylation Assay*

Bead-bound GST-tagged BRCA1 fragments of defined sequence were incubated with 10 pmoles purified human PARP1 (Enzo; ALX-201-063-C020) or PARP3 (Enzo; ALX-201-252-C010) in reaction buffer [50 mmol/L Tris-HCl, pH 7.5, 4 mmol/L $MgCl_2$, 250 μmol/L DTT, 20 mmol/L NaCl, 100 μmol/L NAD, and activated DNA (Trevigen)] at room temperature for 20 minutes. For reactions containing Bio-NAD, 75 μmol/L NAD and 25 μmol/L Bio-NAD were combined and added in reaction buffer solution. Beads were then washed 3 times with washing buffer (55 mmol/L Tris-HCl, pH 7.5, 1 mmol/L EDTA, 200 mmol/L NaCl, 1 mmol/L DTT, 1% Triton X-100) to stop the reaction. Beads were washed once more with 50 mmol/L Tris-HCl, pH 8.0 before GST-tagged proteins were eluted and analyzed.

DNA Binding Assay

Oligonucleotides (sequences available upon request) were labeled using a Biotin 3′ End DNA Labeling kit following manufacturer's instructions (Pierce/Thermo). They were then annealed to generate biotin-conjugated four-way junction DNA structures. GST-F3.7, although still bound to glutathione beads, was PARsylated *in vitro* by PARP1, as described above, or mock treated. After the reaction, beads were washed with GST-binding buffer (55 mmol/L Tris-HCl, pH 7.5, 1 mmol/L EDTA, 200 mmol/L NaCl, 1% Triton X-100, 1 mmol/L DTT, and protease inhibitors) four times before GST-F3.7 or GST was eluted. GST-F3.7 PARsylated by PARP1 or mock treated, or GST, treated similarly, was then incubated with biotinyl four-way junction DNA in DNA-binding buffer (10 mmol/L Tris-HCl, pH = 8.0, 60 mmol/L KCl, 20 μg/mL BSA, 0.1% Triton X-100, 400 μmol/L $MgCl_2$) for 30 minutes at room temperature. Streptavidin M-280 Dynal beads (10 μL; Invitrogen) were then added to each reaction mixture and incubated at room temperature for 10 minutes. Supernatants containing unbound proteins were collected, and the beads were washed four times with DNA-binding buffer before being processed for further analyses.

For PARsylation-driven binding release assays, biotinyl four-way junction DNA-bound F3.7 on Streptavidin beads was incubated with PARP1 in PARP reaction buffer (see above), in the presence and absence of 100 nmol/L olaparib. After the reaction, the supernatant (containing any released protein) and beads (containing remaining bound protein) were collected and analyzed.

Chromosome Analysis

Cells were treated with indicated siRNA or drugs, or transfected with indicated cDNA for 48 hours and then exposed to 150 rad ionizing radiation. Colcemid (30 ng/mL) was added to culture 5 hours after IR, and cells were incubated for an additional 3 hours, collected, and then prepared for analysis of metaphase spreads. Spreads were stained with 4′,6-diamidino-2-phenylindole, dihydrochloride (DAPI).

PDX Breast Cancer Tumor Samples

PDX tumor models were established as described (5). Patient IDs were deidentified to protect confidentiality. Tumor samples were snap-frozen in liquid nitrogen immediately after surgery. Frozen tumor samples were pulverized using a prechilled metal pestle while remaining submerged in liquid nitrogen. Then the vials containing these pulverized samples were slowly removed from the liquid nitrogen bath. Liquid nitrogen evaporated and pulverized tumor tissues remained in the vials and were ready for further processing and analysis. Appropriate amounts of NET-N 400 lysis buffer (400 mmol/L NaCl, 0.5 mmol/L EDTA, 20 mmol/L Tris-HCl, pH 7.5, 0.5% NP-40, 1.5 mmol/L MgCl2, 10% glycerol, 5 mmol/L NEM, 1 μmol/L ADP-HPD, and protease inhibitors) were added to achieve a desired protein concentration in lysates.

Disclosure of Potential Conflicts of Interest

E. Lim reports receiving a commercial cancer research grant from Pfizer. M.J. Eck is a grantee of and consultant to the Novartis Institute for Biomedical Research. R. Scully is a consultant for the Deerfield Institute and reports receiving a commercial research grant from AstraZeneca. D.M. Livingston is a grantee of and consultant to the Novartis Institute for Biomedical Research. No potential conflicts of interest were disclosed by the other authors.

Authors' Contributions

Conception and design: Y. Hu, R. Scully, J.A. Marto, D.M. Livingston
Development of methodology: Y. Hu, S.A. Petit, J.A. Marto
Acquisition of data (provided animals, acquired and managed patients, provided facilities, etc.): Y. Hu, S.A. Petit, K.J. Toomire, A. Xie, E. Lim, S.A. Cao, E. Park, M.J. Eck, M. Brown
Analysis and interpretation of data (e.g., statistical analysis, biostatistics, computational analysis): Y. Hu, S.B. Ficarro, K.J. Toomire, A. Xie, E. Lim, R. Scully
Writing, review, and/or revision of the manuscript: Y. Hu, S.B. Ficarro, E. Lim, M.J. Eck, R. Scully, M. Brown, D.M. Livingston
Administrative, technical, or material support (i.e., reporting or organizing data, constructing databases): Y. Hu, K.J. Toomire, S.A. Cao
Study supervision: Y. Hu, D.M. Livingston
Other (performed mass spectrometry analyses under supervision of J.A. Marto): Y. Hu, S.B. Ficarro

Acknowledgments

The authors thank Drs. Zhao-Qi Wang and Ya Wang for providing *Parp1* knockout MEF cells; Dr. Andrea Richardson for providing human breast cancer samples; AstraZeneca/Kudos for providing a generous initial supply of olaparib; Drs. Guillaume Adelmant and Jean-Bernard Lazaro and members of the Livingston group for numerous helpful discussions and technical advice; and Dr. Daniel Silver for providing some breast cancer cell lines.

Grant Support

This work was supported by grants from the NCI, the Breast Cancer Research Foundation, and the Susan G. Komen Foundation for the Cure (to D.M. Livingston), and by an NCI SPORE grant in breast cancer research to Dana-Farber/Harvard Cancer Center. Y. Hu was supported by a U.S. Department of Defense postdoctoral fellowship award (W81XWH-09-1-0632).

Received November 19, 2013; revised September 10, 2014; accepted September 12, 2014; published OnlineFirst September 24, 2014.

REFERENCES

1. Scully R, Livingston DM. In search of the tumour-suppressor functions of BRCA1 and BRCA2. Nature 2000;408:429–32.
2. Walsh T, King MC. Ten genes for inherited breast cancer. Cancer Cell 2007;11:103–5.
3. Jasin M. Homologous repair of DNA damage and tumorigenesis: the BRCA connection. Oncogene 2002;21:8981–93.
4. Moynahan ME, Chiu JW, Koller BH, Jasin M. Brca1 controls homology-directed DNA repair. Mol Cell 1999;4:511–8.
5. Chen JJ, Silver D, Cantor S, Livingston DM, Scully R. BRCA1, BRCA2, and Rad51 operate in a common DNA damage response pathway. Cancer Res 1999;59:1752s–6s.
6. Venkitaraman AR. Cancer susceptibility and the functions of BRCA1 and BRCA2. Cell 2002;108:171–82.
7. Greenberg RA, Sobhian B, Pathania S, Cantor SB, Nakatani Y, Livingston DM. Multifactorial contributions to an acute DNA damage response by BRCA1/BARD1-containing complexes. Genes Dev 2006;20:34–46.
8. Sobhian B, Shao G, Lilli DR, Culhane AC, Moreau LA, Xia B, et al. RAP80 targets BRCA1 to specific ubiquitin structures at DNA damage sites. Science 2007;316:1198–202.
9. Kim H, Chen J, Yu X. Ubiquitin-binding protein RAP80 mediates BRCA1-dependent DNA damage response. Science 2007;316:1202–5.
10. Wang B, Matsuoka S, Ballif BA, Zhang D, Smogorzewska A, Gygi SP, et al. Abraxas and RAP80 form a BRCA1 protein complex required for the DNA damage response. Science 2007;316:1194–8.
11. Yu X, Chen J. DNA damage-induced cell cycle checkpoint control requires CtIP, a phosphorylation-dependent binding partner of BRCA1 C-terminal domains. Mol Cell Biol 2004;24:9478–86.
12. Coleman KA, Greenberg RA. The BRCA1-RAP80 complex regulates DNA repair mechanism utilization by restricting end resection. J Biol Chem 2011;286:13669–80.
13. Hu Y, Scully R, Sobhian B, Xie A, Shestakova E, Livingston DM. RAP80-directed tuning of BRCA1 homologous recombination

function at ionizing radiation-induced nuclear foci. Genes Dev 2011;25:685–700.
14. Lee I, Blom UM, Wang PI, Shim JE, Marcotte EM. Prioritizing candidate disease genes by network-based boosting of genome-wide association data. Genome Res 2011;21:1109–21.
15. Rajesh C, Baker DK, Pierce AJ, Pittman DL. The splicing-factor related protein SFPQ/PSF interacts with RAD51D and is necessary for homology-directed repair and sister chromatid cohesion. Nucleic Acids Res 2011;39:132–45.
16. Polo SE, Kaidi A, Baskcomb L, Galanty Y, Jackson SP. Regulation of DNA-damage responses and cell-cycle progression by the chromatin remodelling factor CHD4. EMBO J 2010;29:3130–9.
17. Gudjonsson T, Altmeyer M, Savic V, Toledo L, Dinant C, Grofte M, et al. TRIP12 and UBR5 suppress spreading of chromatin ubiquitylation at damaged chromosomes. Cell 2012;150:697–709.
18. Lai JS, Herr W. Ethidium bromide provides a simple tool for identifying genuine DNA-independent protein associations. Proc Natl Acad Sci U S A 1992;89:6958–62.
19. Hatakeyama K, Nemoto Y, Ueda K, Hayaishi O. Purification and characterization of poly(ADP-ribose) glycohydrolase. Different modes of action on large and small poly(ADP-ribose). J Biol Chem 1986;261:14902–11.
20. Wang ZQ, Auer B, Stingl L, Berghammer H, Haidacher D, Schweiger M, et al. Mice lacking ADPRT and poly(ADP-ribosyl)ation develop normally but are susceptible to skin disease. Genes Dev 1995;9:509–20.
21. Shieh WM, Ame JC, Wilson MV, Wang ZQ, Koh DW, Jacobson MK, et al. Poly(ADP-ribose) polymerase null mouse cells synthesize ADP-ribose polymers. J Biol Chem 1998;273:30069–72.
22. Ame JC, Rolli V, Schreiber V, Niedergang C, Apiou F, Decker P, et al. PARP-2, a novel mammalian DNA damage-dependent poly(ADP-ribose) polymerase. J Biol Chem 1999;274:17860–8.
23. Scully R, Chen J, Ochs RL, Keegan K, Hoekstra M, Feunteun J, et al. Dynamic changes of BRCA1 subnuclear location and phosphorylation state are initiated by DNA damage. Cell 1997;90:425–35.
24. Bekker-Jensen S, Lukas C, Kitagawa R, Melander F, Kastan MB, Bartek J, et al. Spatial organization of the mammalian genome surveillance machinery in response to DNA strand breaks. J Cell Biol 2006;173:195–206.
25. Menear KA, Adcock C, Boulter R, Cockcroft XL, Copsey L, Cranston A, et al. 4-[3-(4-cyclopropanecarbonylpiperazine-1-carbonyl)-4-fluorobenzyl]-2H-phth alazin-1-one: a novel bioavailable inhibitor of poly(ADP-ribose) polymerase-1. J Med Chem 2008;51:6581–91.
26. Ogata N, Ueda K, Hayaishi O. ADP-ribosylation of histone H2B. Identification of glutamic acid residue 2 as the modification site. J Biol Chem 1980;255:7610–5.
27. Thakur S, Zhang HB, Peng Y, Le H, Carroll B, Ward T, et al. Localization of BRCA1 and a splice variant identifies the nuclear localization signal. Mol Cell Biol 1997;17:444–52.
28. Chen CF, Li S, Chen Y, Chen PL, Sharp ZD, Lee WH. The nuclear localization sequences of the BRCA1 protein interact with the importin-alpha subunit of the nuclear transport signal receptor. J Biol Chem 1996;271:32863–8.
29. Paull TT, Cortez D, Bowers B, Elledge SJ, Gellert M. Direct DNA binding by Brca1. Proc Natl Acad Sci U S A 2001;98:6086–91.
30. Naseem R, Sturdy A, Finch D, Jowitt T, Webb M. Mapping and conformational characterization of the DNA-binding region of the breast cancer susceptibility protein BRCA1. Biochem J 2006;395:529–35.
31. Simons AM, Horwitz AA, Starita LM, Griffin K, Williams RS, Glover JN, et al. BRCA1 DNA-binding activity is stimulated by BARD1. Cancer Res 2006;66:2012–8.
32. Sturdy A, Naseem R, Webb M. Purification and characterisation of a soluble N-terminal fragment of the breast cancer susceptibility protein BRCA1. J Mol Biol 2004;340:469–75.
33. Hassa PO, Haenni SS, Elser M, Hottiger MO. Nuclear ADP-ribosylation reactions in mammalian cells: where are we today and where are we going? Microbiol Mol Biol Rev 2006;70:789–829.
34. Krishnakumar R, Kraus WL. The PARP side of the nucleus: molecular actions, physiological outcomes, and clinical targets. Mol Cell 2010;39:8–24.
35. Hassa PO, Hottiger MO. The diverse biological roles of mammalian PARPS, a small but powerful family of poly-ADP-ribose polymerases. Front Biosci 2008;13:3046–82.
36. Ramirez CJ, Fleming MA, Potter JD, Ostrander GK, Ostrander EA. Marsupial BRCA1: conserved regions in mammals and the potential effect of missense changes. Oncogene 2004;23:1780–8.
37. Fleming MA, Potter JD, Ramirez CJ, Ostrander GK, Ostrander EA. Understanding missense mutations in the BRCA1 gene: an evolutionary approach. Proc Natl Acad Sci U S A 2003;100:1151–6.
38. Wu LC, Wang ZW, Tsan JT, Spillman MA, Phung A, Xu XL, et al. Identification of a RING protein that can interact in vivo with the BRCA1 gene product. Nat Genet 1996;14:430–40.
39. Kim H, Huang J, Chen J. CCDC98 is a BRCA1-BRCT domain-binding protein involved in the DNA damage response. Nat Struct Mol Biol 2007;14:710–5.
40. Liu Z, Wu J, Yu X. CCDC98 targets BRCA1 to DNA damage sites. Nat Struct Mol Biol 2007;14:716–20.
41. Alvarez-Gonzalez R, Althaus FR. Poly(ADP-ribose) catabolism in mammalian cells exposed to DNA-damaging agents. Mut Res 1989;218:67–74.
42. Schreiber V, Dantzer F, Ame JC, de Murcia G. Poly(ADP-ribose): novel functions for an old molecule. Nat Rev Mol Cell Biol 2006;7:517–28.
43. Pleschke JM, Kleczkowska HE, Strohm M, Althaus FR. Poly(ADP-ribose) binds to specific domains in DNA damage checkpoint proteins. J Biol Chem 2000;275:40974–80.
44. Stilmann M, Hinz M, Arslan SC, Zimmer A, Schreiber V, Scheidereit C. A nuclear poly(ADP-ribose)-dependent signalosome confers DNA damage-induced IkappaB kinase activation. Mol Cell 2009;36:365–78.
45. Haince JF, Kozlov S, Dawson VL, Dawson TM, Hendzel MJ, Lavin MF, et al. Ataxia telangiectasia mutated (ATM) signaling network is modulated by a novel poly(ADP-ribose)-dependent pathway in the early response to DNA-damaging agents. J Biol Chem 2007;282:16441–53.
46. Panzeter PL, Realini CA, Althaus FR. Noncovalent interactions of poly(adenosine diphosphate ribose) with histones. Biochemistry 1992;31:1379–85.
47. Yan J, Kim YS, Yang XP, Li LP, Liao G, Xia F, et al. The ubiquitin-interacting motif containing protein RAP80 interacts with BRCA1 and functions in DNA damage repair response. Cancer Res 2007;67:6647–56.
48. Rouet P, Smih F, Jasin M. Introduction of double-strand breaks into the genome of mouse cells by expression of a rare-cutting endonuclease. Mol Cell Biol 1994;14:8096–106.
49. Xia B, Sheng Q, Nakanishi K, Ohashi A, Wu J, Christ N, et al. Control of BRCA2 cellular and clinical functions by a nuclear partner, PALB2. Mol Cell 2006;22:719–29.
50. Schultz N, Lopez E, Saleh-Gohari N, Helleday T. Poly(ADP-ribose) polymerase (PARP-1) has a controlling role in homologous recombination. Nucleic Acids Res 2003;31:4959–64.
51. Yang YG, Cortes U, Patnaik S, Jasin M, Wang ZQ. Ablation of PARP-1 does not interfere with the repair of DNA double-strand breaks, but compromises the reactivation of stalled replication forks. Oncogene 2004;23:3872–82.
52. Shen Y, Rehman FL, Feng Y, Boshuizen J, Bajrami I, Elliott R, et al. BMN 673, a novel and highly potent PARP1/2 inhibitor for the treatment of human cancers with DNA repair deficiency. Clin Can Res 2013;19:5003–15.
53. Puget N, Knowlton M, Scully R. Molecular analysis of sister chromatid recombination in mammalian cells. DNA Repair 2005;4:149–61.
54. Nagaraju G, Odate S, Xie A, Scully R. Differential regulation of short- and long-tract gene conversion between sister chromatids by Rad51C. Mol Cell Biol 2006;26:8075–86.
55. Bouwman P, Aly A, Escandell JM, Pieterse M, Bartkova J, van der Gulden H, et al. 53BP1 loss rescues BRCA1 deficiency and is associated with triple-negative and BRCA-mutated breast cancers. Nat Struc Mol Biol 2010;17:688–95.
56. Bunting SF, Callen E, Wong N, Chen HT, Polato F, Gunn A, et al. 53BP1 inhibits homologous recombination in Brca1-deficient cells by blocking resection of DNA breaks. Cell 2010;141:243–54.

57. Baumann P, Benson FE, West SC. Human Rad51 protein promotes ATP-dependent homologous pairing and strand transfer reactions in vitro. Cell 1996;87:757–66.
58. Zhu Z, Chung WH, Shim EY, Lee SE, Ira G. Sgs1 helicase and two nucleases Dna2 and Exo1 resect DNA double-strand break ends. Cell 2008;134:981–94.
59. Bhattacharyya A, Ear US, Koller BH, Weichselbaum RR, Bishop DK. The breast cancer susceptibility gene BRCA1 is required for subnuclear assembly of Rad51 and survival following treatment with the DNA cross-linking agent cisplatin. J Biol Chem 2000;275:23899–903.
60. Tomimatsu N, Mukherjee B, Deland K, Kurimasa A, Bolderson E, Khanna KK, et al. Exo1 plays a major role in DNA end resection in humans and influences double-strand break repair and damage signaling decisions. DNA Repair 2012;11:441–8.
61. Pathania S, Nguyen J, Hill SJ, Scully R, Adelmant GO, Marto JA, et al. BRCA1 is required for postreplication repair after UV-induced DNA damage. Mol Cell 2011;44:235–51.
62. Schlacher K, Wu H, Jasin M. A distinct replication fork protection pathway connects Fanconi anemia tumor suppressors to RAD51-BRCA1/2. Cancer Cell 2012;22:106–16.
63. Neve RM, Chin K, Fridlyand J, Yeh J, Baehner FL, Fevr T, et al. A collection of breast cancer cell lines for the study of functionally distinct cancer subtypes. Cancer Cell 2006;10:515–27.
64. Elstrodt F, Hollestelle A, Nagel JH, Gorin M, Wasielewski M, van den Ouweland A, et al. BRCA1 mutation analysis of 41 human breast cancer cell lines reveals three new deleterious mutants. Cancer Res 2006;66:41–5.
65. Ding L, Ellis MJ, Li S, Larson DE, Chen K, Wallis JW, et al. Genome remodelling in a basal-like breast cancer metastasis and xenograft. Nature 2010;464:999–1005.
66. DeRose YS, Wang G, Lin YC, Bernard PS, Buys SS, Ebbert MT, et al. Tumor grafts derived from women with breast cancer authentically reflect tumor pathology, growth, metastasis and disease outcomes. Nat Med 2011;17:1514–20.
67. Landis MD, Lehmann BD, Pietenpol JA, Chang JC. Patient-derived breast tumor xenografts facilitating personalized cancer therapy. Breast Cancer Res 2013;15:201.
68. Dimitrov SD, Lu D, Naetar N, Hu Y, Pathania S, Kanellopoulou C, et al. Physiological modulation of endogenous BRCA1 p220 abundance suppresses DNA damage during the cell cycle. Genes Dev 2013;27:2274–91.
69. Helleday T. The underlying mechanism for the PARP and BRCA synthetic lethality: clearing up the misunderstandings. Mol Oncol 2011;5:387–93.
70. Murai J, Huang SY, Das BB, Renaud A, Zhang Y, Doroshow JH, et al. Trapping of PARP1 and PARP2 by clinical PARP inhibitors. Cancer Res 2012;72:5588–99.
71. Bryant HE, Schultz N, Thomas HD, Parker KM, Flower D, Lopez E, et al. Specific killing of BRCA2-deficient tumours with inhibitors of poly(ADP-ribose) polymerase. Nature 2005;434:913–7.
72. Farmer H, McCabe N, Lord CJ, Tutt AN, Johnson DA, Richardson TB, et al. Targeting the DNA repair defect in BRCA mutant cells as a therapeutic strategy. Nature 2005;434:917–21.
73. Ledermann J, Harter P, Gourley C, Friedlander M, Vergote I, Rustin G, et al. Olaparib maintenance therapy in platinum-sensitive relapsed ovarian cancer. N Engl J Med 2012;366:1382–92.
74. Liu JF, Tolaney SM, Birrer M, Fleming GF, Buss MK, Dahlberg SE, et al. A Phase 1 trial of the poly(ADP-ribose) polymerase inhibitor olaparib (AZD2281) in combination with the anti-angiogenic cediranib (AZD2171) in recurrent epithelial ovarian or triple-negative breast cancer. Eur J Cancer 2013;49:2972–8.
75. Rebbeck TR, Mitra N, Domchek SM, Wan F, Friebel TM, Tran TV, et al. Modification of BRCA1-associated breast and ovarian cancer risk by BRCA1-interacting genes. Cancer Res 2011;71:5792–805.
76. Antoniou AC, Wang X, Fredericksen ZS, McGuffog L, Tarrell R, Sinilnikova OM, et al. A locus on 19p13 modifies risk of breast cancer in BRCA1 mutation carriers and is associated with hormone receptor-negative breast cancer in the general population. Nat Genet 2010;42:885–92.
77. Bolton KL, Tyrer J, Song H, Ramus SJ, Notaridou M, Jones C, et al. Common variants at 19p13 are associated with susceptibility to ovarian cancer. Nat Genet 2010;42:880–4.
78. Nikkila J, Coleman KA, Morrissey D, Pylkas K, Erkko H, Messick TE, et al. Familial breast cancer screening reveals an alteration in the RAP80 UIM domain that impairs DNA damage response function. Oncogene 2009;28:1843–52.
79. Solyom S, Aressy B, Pylkas K, Patterson-Fortin J, Hartikainen JM, Kallioniemi A, et al. Breast cancer-associated Abraxas mutation disrupts nuclear localization and DNA damage response functions. Sci Transl Med 2012;4:122ra23.
80. Solyom S, Patterson-Fortin J, Pylkas K, Greenberg RA, Winqvist R. Mutation screening of the MERIT40 gene encoding a novel BRCA1 and RAP80 interacting protein in breast cancer families. Breast Cancer Res Treat 2010;120:165–8.
81. Weigman VJ, Chao HH, Shabalin AA, He X, Parker JS, Nordgard SH, et al. Basal-like breast cancer DNA copy number losses identify genes involved in genomic instability, response to therapy, and patient survival. Breast Cancer Res Treat 2012;133:865–80.
82. Wu J, Liu C, Chen J, Yu X. RAP80 protein is important for genomic stability and is required for stabilizing BRCA1-A complex at DNA damage sites in vivo. J Biol Chem 2012;287:22919–26.
83. Yin Z, Menendez D, Resnick MA, French JE, Janardhan KS, Jetten AM. RAP80 is critical in maintaining genomic stability and suppressing tumor development. Cancer Res 2012;72:5080–90.
84. Castillo A, Paul A, Sun B, Huang TH, Wang Y, Yazinski SA, et al. The BRCA1-interacting protein abraxas is required for genomic stability and tumor suppression. Cell Rep 2014;8:807–17.
85. Xie A, Puget N, Shim I, Odate S, Jarzyna I, Bassing CH, et al. Control of sister chromatid recombination by histone H2AX. Mol Cell 2004;16:1017–25.

ARP1-Driven Poly-ADP-Ribosylation Regulates BRCA1 Function n Homologous Recombination–Mediated DNA Repair

duo Hu, Sarah A. Petit, Scott B. Ficarro, et al.

ancer Discovery 2014;4:1430-1447. Published OnlineFirst September 24, 2014.